Available online at www.sciencedirect.com
ScienceDirect
International Journal of Solids and Structures 44 (2007) 5075–5100
INTERNATIONAL JOURNAL OF SOLIDS and STRUCTURES
www.elsevier.com/locate/ijsolstr

Analysis of creep deformation and creep damage in thin-walled branched shells from materials with different behavior in tension and compression

A. Zolochevsky [a], A. Galishin [b], S. Sklepus [c], G.Z. Voyiadjis [d,*]

[a] Department of Materials Technology, Chemistry block II, Norwegian University of Science and Technology, Sem Sælandsvei 12, Trondheim N-7491, Norway
[b] Department of Thermoplasticity, The Timoshenko Institute of Mechanics, Nesterova 3, 03057 Kiev, Ukraine
[c] Department of Applied Mathematics and Calculation Methods, Institute of Mechanical Engineering Problems, Pozharsky 2/ 10, 61046 Kharkov, Ukraine
[d] Department of Civil and Environmental Engineering, Louisiana State University, Baton Rouge, LA 70803, USA

Received 7 October 2006; received in revised form 4 December 2006
Available online 22 December 2006

Abstract

A constitutive model for describing the creep and creep damage in initially isotropic materials with different properties in tension and compression has been applied to the modeling of creep deformation and creep damage growth in thin-walled shells of revolution with the branched meridian. The approach of establishing the basic equations for axisymmetrically loaded branched shells under creep deformation and creep damage conditions has been introduced. To solve the initial/boundary-value problem, the fourth-order Runge–Kutta–Merson's method of time integration with the combination of the numerically stable Godunov's method of discrete orthogonalization is used. The solution of the boundary value problem for the branched shell at each time instant is reduced to integration of the series of systems of ordinary differential equations describing the deformation of each branch and the shell with basic meridian. Some numerical examples are considered, and the processes of creep deformation and creep damage growth in a shell with non-branched meridian as well as in a branched shell are analyzed. The influence of the tension–compression asymmetry on the stress–strain state and damage evolution in a shell with non-branched meridian as well as in a branched shell with time are discussed.

Keywords: Constitutive equation; Creep; Creep damage; Asymmetric effect; Branched shell

1. Introduction

Polycrystalline materials subjected to loadings at elevated temperature for a prolonged period of time exhibit creep deformation considered as a time-dependent irreversible deformation process. In the initial

* Corresponding author. Tel.: +1 225 578 8668; fax: +1 225 578 9176.
E-mail address: voyiadjis@eng.lsu.edu (G.Z. Voyiadjis).

0020-7683/$ - see front matter © 2006 Elsevier Ltd. All rights reserved.
doi:10.1016/j.ijsolstr.2006.12.019

stages of the creep process in polycrystalline materials, dislocations, impurity atoms and voids accumulate at the grain boundaries to form grain boundary cavitation (Ashby and Brown, 1983; Evans, 1984; Riedel, 1987). As microscopic cavities at the grain boundaries get larger and coalesce, dislocations, impurity atoms and voids move out to grain boundaries, and microcracks along the grain facets begin to be formed. Growth and coalescence of these microcracks lead to the creep rupture in the final stage of the creep process with formation of macrocrack with some preferential orientation related to the loading conditions, for example, direction perpendicular to the maximum principal stress or the principal shear direction (Chen and Argon, 1981; Hayhurst, 1972; Hayhurst et al., 1980; Sakane and Tokura, 2002). Thus, creep deformation changes the microstructure of polycrystalline materials by introducing dislocations, impurity atoms and voids in the initial stages, microscopic cavities in the following, and microcracks in the final stage of the creep process, all of them, at the grain boundaries with some preferential orientation related to the loading conditions. Furthermore, the velocity of the growth of already existing grain boundary microscopic cavities and microcracks, and of the nucleation of new ones essentially depends on the intensity of creep deformation. On the other hand, creep deformation of materials is influenced by the growth of microscopic cavities and microcracks. This influence begins at the primary and secondary stages of the creep process, and becomes visible in the tertiary stage due to an increase of the creep strain rate, preceding the creep rupture. Thus, creep deformation and material deterioration due to growth of creep damage occur parallel to each other, and they have a reciprocal effect.

One of the creep features of a large class of polycrystalline materials (light alloys, gray cast irons, high-strength steels, ceramic polycrystals, etc.) is their different behavior in tension and compression (Altenbach et al., 1995; El-Shennawy et al., 1999; Gorev et al., 1978, 1979; Hostert, 1975; Khojasteh-Vahabzadeh, 1991; Lucas and Pelloux, 1981; Nechtelberger, 1985; Nikitenko et al., 1971; Ohashi et al., 1982; Pintschovius et al., 1989; Rabotnov, 1969; Rix, 1997; Rubanov, 1987; Sosnin, 1970; Tilly and Harrison, 1972; Tsvelodub, 1991; Wereszczak et al., 1999; Zolochevskii, 1982, 1988). This creep feature may be investigated experimentally by comparing creep curves obtained from uniaxial tests in tension and compression at the same temperature and taking specimens at the same orientation from the body under consideration. In this way it is established for many polycrystalline materials that the absolute values of creep strain, chosen for one and the same absolute value of constant stress, and for one and the same value of time, are essentially different depending on the sign of the stress. Thus, one has two different creep curves (one in tension, and the other in compression).

The changes of the microstrucutre in polycrystalline materials that result from the creep deformation need to be also quantified under uniaxial tension and uniaxial compression. Analysis of the creep damage growth under uniaxial tension in polycrystalline materials has been presented (Kassner and Hayes, 2003) by considering the appearance and growth of microscopic cavities (Fig. 1) and wedge microcracks (Fig. 2) along grain boundaries located perpendicular to the axis of tensile loading. On the other hand, the creep damage growth under uniaxial compression in ceramics has been related to the nucleation, growth and coalescence of cavities (Fig. 3) in glassy grain boundary phases which are parallel to the compressive loading axis as well as to the possible nucleation and growth in the following of microcracks formed at such grain boundary faces (Chan et al., 1984; Page et al., 1984). Thus, the creep damage depends on the stress state type and has the directional nature. In the general case, it is possible to assume that creep damage growth occurs at the grain boundaries located perpendicular to the direction of the maximum principal stress (Cocks and Ashby, 1982; Needleman and Rice, 1983; Tvergaard, 1984).

As an example, Fig. 4a–c shows the growth of the specific dissipation energy φ with time t up to creep rupture in an aluminum alloy AK4-1T at the temperature of 473 K (Gorev et al., 1978; Rubanov, 1987) under

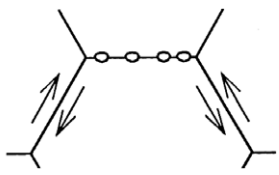

Fig. 1. A schematic of the cavitating grain boundary located perpendicular to the axis of tensile loading in association with grain boundary sliding.

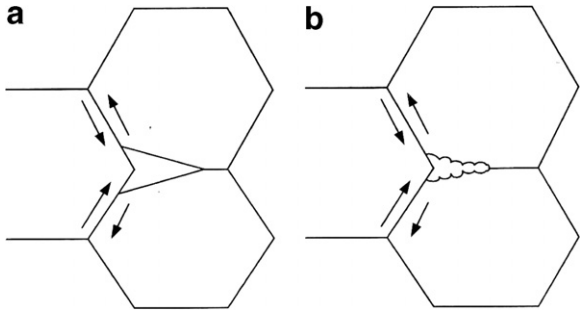

Fig. 2. A schematic of the grain facets located perpendicular to the axis of tensile loading with a wedge microcrack (a) formed at grain boundary triple points in association with grain boundary sliding, and with a wedge microcrack (b) as an accumulation of microscopic cavities (Kassner and Hayes, 2003).

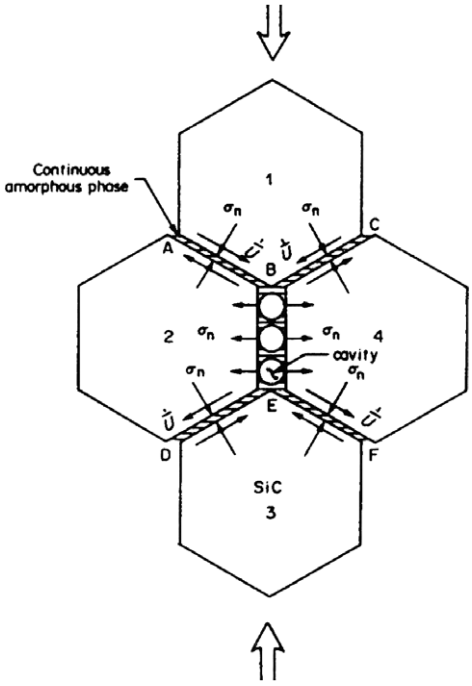

Fig. 3. A schematic of the cavitating grain boundary, BE, located parallel to the axis of compressive loading with illustration of the sliding rate and normal stresses on adjacent grain boundaries (Chan et al., 1984).

uniaxial tension (a), uniaxial compression (b) and pure torsion (c). Here the specific dissipation energy due to damage is expressed as

$$\varphi = \int_0^t \sigma_{kl}\dot{p}_{kl}\mathrm{d}t \tag{1}$$

where σ_{kl} is the stress tensor, p_{kl} is the creep strain tensor, and the dot above the symbol denotes a derivative with respect to time. It is seen from Fig. 4(a) and (b) that the maximum difference in creep behavior of an aluminum alloy AK4-1T at 473 K between tension and compression is related to the third stage of the creep curves. For example, the difference in the creep strain rate in the secondary stage of the creep curves for tension and compression is different by a factor of about two, whist the corresponding creep rupture times are different by a factor of about three. This picture of the creep behavior of the material under consideration can be explained taking into account an orientation-dependent character of microstructural changes during

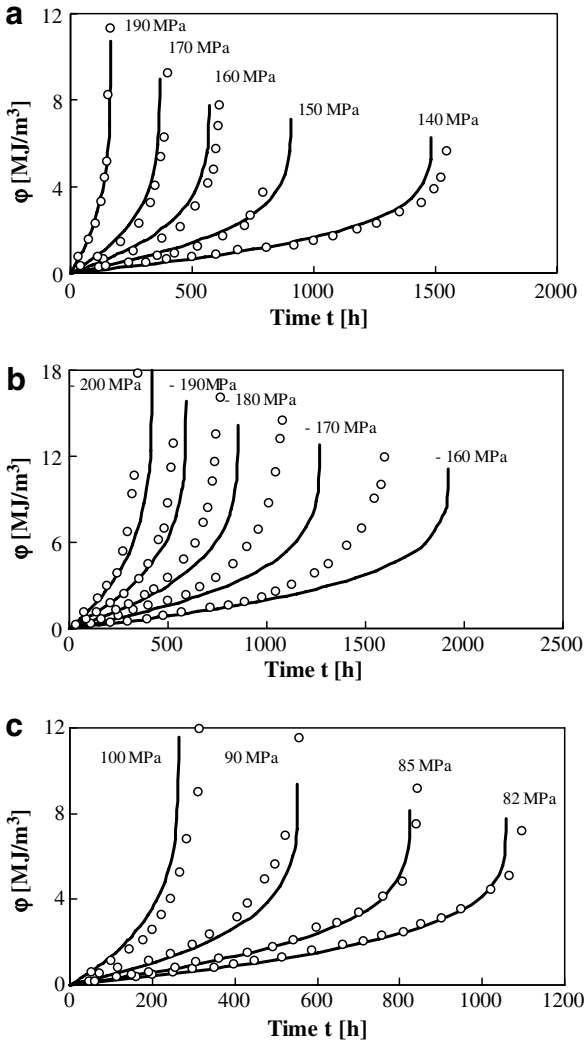

Fig. 4. Variation of the specific dissipation energy with time of an aluminum alloy AK4-1T at the temperature of 473 K under uniaxial tension (a), uniaxial compression (b) and pure torsion (c). Experimental data are denoted by circles, while solid lines are the analogous theoretical results.

dislocation creep and for the directional nature of creep damage. In the case of uniaxial tension microstructural changes tend to evolve and propagate at the grain boundaries located perpendicular to the axis of loading (active damage state).

On the other hand, under uniaxial compression microstructural changes in an aluminum alloy develop at the grain boundaries located parallel to the axis of loading (passive damage state). Thus, the velocity of the damage growth under uniaxial compression is much smaller in comparison with the magnitude under uniaxial tension, i.e. there exists a unilateral nature of the creep damage.

An aluminum alloy AK4-1T at 473 K is initially an isotropic material under creep conditions. This fact was established on the basis of creep tests conducted on specimens taken from the three principal directions of the AK4-1T plate as well as on specimens oriented at an angle of $\pi/4$ with respect to the longitudinal and transverse directions (Rubanov, 1987). One introduces the stress intensity

$$\sigma_i = \sqrt{\frac{3}{2} s_{kl} s_{kl}} \tag{2}$$

where s_{kl} is the stress deviator, $s_{kl} = \sigma_{kl} - \frac{1}{3} I_1 \delta_{kl}$, I_1 is the first invariant of the stress tensor, $I_1 = \sigma_{kl}\delta_{kl}$, and δ_{kl} is the Kronecker delta. It is seen from Fig. 4(a–c) that at the same absolute value of the stress intensity in Eq. (2) and at any given time, the specific dissipation energy given by expression (1) is largest under pure torsion and smallest under uniaxial compression. This also indicates the largest degree of the creep damage is in pure torsion. Thus, the creep deformation and damage development in the light alloy under consideration must be described by independent laws under conditions of pure torsion. Obviously, it is necessary to have the results of three series of the creep tests (uniaxial tension, uniaxial compression and pure torsion) to describe the creep deformation of an aluminum alloy AK4-1T at 473 K up to creep rupture. Note that the creep behavior of this light alloy has been broadly discussed by Altenbach et al. (1995), Altenbach and Zolochevsky (1991), Betten (2002), Betten et al. (1998, 1999, 2003), Kawai (2002), Mahnken (2003), Tsvelodub (1991), Voyiadjis and Zolochevsky (2000), Zolochevskii (1982), Zolochevsky (1982, 1991), Zolochevsky and Obataya (2001), and Zolochevsky and Voyiadjis (2005).

In the papers by Betten et al. (1998, 1999, 2003), Voyiadjis and Zolochevsky (2000), Zolochevsky and Obataya (2001), and Zolochevsky and Voyiadjis (2005) a creep theory for initially isotropic polycrystalline materials under multiaxial loading was recently proposed and discussed which is able to reproduce simultaneously different creep properties and different damage development in tension, compression and torsion. Note that a damage variable can be introduced into the consideration as the scalar, vector or tensor of different ranks. Consideration in the creep theory by Betten et al. (1998, 1999, 2003), Voyiadjis and Zolochevsky (2000), Zolochevsky and Obataya (2001), and Zolochevsky and Voyiadjis (2005) of the scalar damage parameter in a form of the specific dissipation energy simultaneously with putting into the expression for the equivalent stress an eigenvector associated with the maximum principal stress which often coincides with the direction of the maximum damage gives the possibility to describe the experimental results under uniaxial non-proportional, multiaxial proportional, and multiaxial non-proportional loadings for both isothermal and non-isothermal processes in the primary, secondary, and tertiary creep states of various polycrystalline materials. In this way, a good correlation has been obtained between the results generated from the proposed creep theory and the experimental data for one-, two- and three-dimensional stress states.

The aim of the present paper is the application of such a creep theory to the modeling of creep deformation and creep damage in thin-walled branched shells. The present paper will not consider the movement of the front of creep rupture in shells, the creep damage localization and the creep buckling of shells.

In the past, various authors have considered the formulation and solution of numerous boundary value problems to analyze the creep deformation and creep damage growth in thin-walled shells. However, they assumed the same creep deformation and same creep damage development in tension and compression for the materials of shells (Altenbach and Naumenko, 1997; Hayhurst, 1981; Hyde et al., 2003; Kojic and Bathe, 1987; Miuazaki, 1987; Morachkovskii and Zolochevskii, 1980; Penny and Marriott, 1995; Rabotnov, 1969; Shariyat and Eslami, 1996; Sichov, 1998, 2003; Takezono and Fujioka, 1981; Zolochevskii and Morachkovskii, 1982; Zolochevsky and Morachkovsky, 1978, 1979). For the first time, the creep deformation of shells with non-branched meridian taking into account different behavior of materials in tension and compression has been analyzed by Zolochevsky (1980, 1982), and subsequently by Betten and Borrmann (1987) and Altenbach and Zolochevsky (1991). However, to the best of the authors' knowledge, up to now no investigations exist of creep deformation and creep damage development in branched shells composed of materials with different behavior in tension and compression. This class of problems is particularly important because branched axisymmetric shells are used in chemical, nuclear, aircraft and space facilities at high temperatures and under severe operational and accidental conditions for which the anti-symmetric behavior in tension and compression is a significant feature.

2. Constitutive model

One considers a creep theory (Betten et al., 1998; Voyiadjis and Zolochevsky, 2000) for initially isotropic polycrystalline materials, in which creep damage is related to dislocation creep and microstructural changes at the grain boundaries which are orthogonal to the direction of the maximum principal stress. Creep strains are assumed to be small.

The expression for the equivalent stress σ_e, setting the equivalence of uniaxial and multiaxial stress states, is determined as

$$\sigma_e = \sigma_2 + \alpha\sigma_1 \tag{3}$$

where

$$\sigma_1 = C\sigma_{\max},\ \sigma_{\max} = \sigma_{kl}m_k m_l$$
$$\sigma_2 = \sqrt{AI_1^2 + BI_2} \tag{4}$$

$\sigma_{\max}$ is the maximum principal stress, I_2 is the second invariant of the stress tensor, $I_2 = \sigma_{kl}\sigma_{kl}$, α is a weight coefficient which takes into account the contribution of the linear scalar function σ_1 into expression (3), A, B and C are material parameters dependent on the temperature, and $\mathbf{m} = \{m_k\}_{k=1}^3$ is an eigenvector associated with the maximum principal stress.

A number of comments need to be made in reference to Eqs. (3) and (4). First, the representation in Eq. (3) of the equivalent stress consists of two terms that are determined by the simultaneous action of the two creep mechanisms. The first term, which reduces to the stress intensity under the first and second conditions in Eq. (5), represents the generalization of the stress intensity in the case of compressible materials under creep conditions and models the influence of the movement of dislocations on the creep behavior. The second one in Eq. (3) reflects the effect of microstructural changes at the grain faces on the creep behavior and gives the opportunity to describe different creep properties in tension and compression, damage induced anisotropy, and different damage development for tension and compression.

Second, expression (3) contains three material parameters (A, B and αC) as well as the linear and quadratic scalar functions σ_1 and σ_2^2. Introduction of the cubic scalar function into the expression of the equivalent stress is principally given in the papers by Betten et al. (1999, 2003) and Zolochevsky and Obataya (2001). It was shown (Betten et al., 1998; Voyiadjis and Zolochevsky, 2000) that the results generated from the creep theory based on the equivalent stress with linear and quadratic scalar functions and without a cubic scalar function are in good correlation with the experimental data for two-dimensional stress states.

Third, the weight coefficient α is introduced in Eq. (3) for convenience only. It is impossible to find the coefficient α separately from the parameter C. Expression (3) includes as particular cases a number of expressions well known in the literature. For example, it is not difficult to see that under conditions

$$A = -\frac{1}{2},\ B = \frac{3}{2},\ \alpha = 0 \tag{5}$$

expressions (3) and (4) include as a particular case the expression for the equivalent stress

$$\sigma_e = \sigma_i \tag{6}$$

in the well-known Huber-von Mises-type potential based on the stress intensity given by Eq. (2) for the case of isotropic materials with the same behavior in tension and compression.

The constitutive equation for creep deformation of the materials with different behaviors in tension and compression has the following structure (Betten et al., 1998; Voyiadjis and Zolochevsky, 2000):

$$\dot{p}_{kl} = \frac{\sigma_e^m \varphi^{-\beta}}{\left(1 - \frac{\varphi}{\varphi_*}\right)^q}\left(\frac{AI_1\delta_{kl} + B\sigma_{kl}}{\sigma_2} + \alpha C m_k m_l\right) \tag{7}$$

where m, β and q are material parameters. The specific dissipation energy φ given by expression (1) is taken in Eq. (7) as the cumulative damage parameter. During the process of creep one has $\varphi \in [0,\varphi_*]$. An initial value $\varphi = 0$ corresponds to a reference state while a critical value $\varphi = \varphi_*$ corresponds to creep rupture time. Note that uses of the function $\varphi^{-\beta}$ in Eq. (7) at $t = 0$ leads to the infinite creep strain rates. For the description of creep for small values of time it is necessary by analogy with the traditional creep theories (Betten, 2002; Rabotnov, 1969) to do the transition from the creep hardening model based on Eq. (7) with the specific dissipation energy φ and the function $\varphi^{-\beta}$ to the equivalent creep model with time hardening where some power function of time will be used instead of $\varphi^{-\beta}$. On the other hand, the exponential relation $\exp(-\gamma\varphi)$ with material parameter γ is more convenient to use in Eq. (7) instead of the function $\varphi^{-\beta}$.

Using Eqs. (1), (3), (4) and (7) one arrives at the following damage growth equation

$$\dot{\varphi} = \frac{\sigma_e^{m+1}\varphi^{-\beta}}{\left(1-\frac{\varphi}{\varphi_*}\right)^q} \tag{8}$$

Considering data of basic experiments such as uniaxial tension with the vector $\mathbf{m} = \{1,0,0\}^{\mathrm{T}}$

$$\dot{p}_{11} = \frac{K_+\sigma_{11}^m\varphi^{-\beta}}{\left(1-\frac{\varphi}{\varphi_*}\right)^q},\ \ \varphi = \sigma_{11}p_{11} \tag{9}$$

uniaxial compression with $\mathbf{m} = \{0,1,0\}^{\mathrm{T}}$

$$\dot{p}_{11} = -\frac{K_-|\sigma_{11}|^m\varphi^{-\beta}}{\left(1-\frac{\varphi}{\varphi_*}\right)^q},\ \ \varphi = \sigma_{11}p_{11} \tag{10}$$

and pure torsion with the vector $\mathbf{m} = \{1/\sqrt{2}, 1/\sqrt{2}, 0\}^{\mathrm{T}}$

$$2\dot{p}_{12} = \frac{K_0\sigma_{12}^m\varphi^{-\beta}}{\left(1-\frac{\varphi}{\varphi_*}\right)^q},\ \ \varphi = 2\sigma_{12}p_{12} \tag{11}$$

and using material constants K_+, K_-, K_0, m, β and q, it is possible to determine the material parameters in Eqs. (7) and (8) of the constitutive model as follows (Betten et al., 1998; Voyiadjis and Zolochevsky, 2000):

$$\begin{aligned} \alpha C &= K_+^{\frac{1}{m+1}} - K_-^{\frac{1}{m+1}} \\ \sqrt{2B} &= K_0^{\frac{1}{m+1}} - \alpha C \\ A &= K_-^{\frac{2}{m+1}} - B \end{aligned} \tag{12}$$

The superscript 'T' above denotes the transposition operation.

If the results from a set of basic experiments show that

$$K_- = K_+,\ \ K_0 = 3^{\frac{m+1}{2}}K_+ \tag{13}$$

then together with Eq. (12) one has

$$B = \frac{3}{2}K_+^{\frac{2}{m+1}},\quad \alpha C = 0,\quad A = -\frac{1}{3}B \tag{14}$$

Using then Eqs. (2)–(4), (7), (8) and (14) it is not difficult to obtain

$$\dot{p}_{kl} = \frac{\left(\sqrt{\frac{2}{3}B}\sigma_i\right)^m\varphi^{-\beta}}{\left(1-\frac{\varphi}{\varphi_*}\right)^q}\sqrt{\frac{3}{2}B}\frac{s_{kl}}{\sigma_i} \tag{15}$$

$$\dot{\varphi} = \frac{\left(\sqrt{\frac{2}{3}B}\sigma_i\right)^{m+1}\varphi^{-\beta}}{\left(1-\frac{\varphi}{\varphi_*}\right)^q}$$

According to Rabotnov (1969), the alternative damage parameter $\omega \in [0,1]$ may be defined as the microstructural change area density or net area reduction in the observed plane. An initial value $\omega = 0$ corresponds to a reference state while a critical value $\omega = \omega_* = 1$ corresponds to creep rupture time. One assumes that there exists such a connection between the two damage parameters under consideration as $\omega = \varphi/\varphi_*$. Then it is not difficult to see that the value $\varphi = 0$ at a reference state corresponds to the value $\omega = 0$ while the critical value $\varphi = \varphi_*$ at the instant of creep rupture time corresponds to the critical value $\omega = \omega_* = 1$. Introducing new material constants $A_1 = \left(\sqrt{\frac{2}{3}B}\right)^{m+1}$ and $D_1 = \frac{A_1}{\varphi_*}$, Eq. (15), for example, in the case of $\varphi = \varphi_* = \text{const}$

can be rewritten as $\dot{p}_{kl} = \frac{3}{2} A_1 \frac{\sigma_i^m \varphi^{-\beta}}{(1-\omega)^q} \frac{s_{kl}}{\sigma_i}$, $\dot{\omega} = D_1 \frac{\sigma_i^{m+1} \varphi^{-\beta}}{(1-\omega)^q}$. Obviously, last equations can be considered as a particular case of the general creep theory by Rabotnov (1969) with the specific dissipation energy φ as a measure of the creep hardening and with scalar damage parameter ω for the traditional damaged materials with characteristics, which are independent of the kind of loading. Eq. (15) will be used in the following analyses of the creep deformation in a thin-walled shell made from a material with the same behavior in tension and compression to test the proposed below numerical integration algorithm against the numerical data by Takezono and Fujioka (1981) based on the power function of the hardening measure in the creep description.

3. Governing equations for branched shell under creep conditions

One considers a shell of revolution (Fig. 5) such that the meridian of the surface corresponds to the meridian of the basic shell with K branch nodes. The number of open-branch meridians that converge at each node i be defined by M_i $(0 \leqslant i \leqslant K)$. In Fig. 5 the meridians of branches that converge at the node k are numbered, for example, from one up to $M_k = 5$. One introduces in the plane of the branched shell (Fig. 5) the axis of rotation z and distance r of one of the meridian points from the axis of rotation. Each branch can be considered as a thin shell of revolution consisting of elements with a different geometry. The position of an arbitrary point of the basic shell and each branch may be determined in the local (to basic shell or branch) orthogonal curvilinear coordinate system x_i $(i = 1, 2, 3)$, where x_1 and x_2 are coordinates of the middle surface; x_1 $(x_{10} \leqslant x_1 \leqslant x_{1N})$ is the length of the coordinate meridian arc referenced from the non-node end $x_1 = x_{10}$; x_2 is the circumferential coordinate; x_3 $(-h/2 \leqslant x_3 \leqslant h/2)$ is the distance of the point from the coordinate surface referenced in the direction of the outer normal; and $h = h(x_1)$ is the thickness of the branch or basic shell.

One assumes that the branched shell is initially unstressed and undeformed at a temperature T_0, and it is then subjected to an axisymmetrically and statically applied thermal and force loading. One will now consider the basic equations for each branch as well as for the shell with the basic meridian in the frame of the Kirchhoff–Love's hypotheses and under the assumption that the strains of the coordinate surface as well as the square of rotation angle of the normal are small compared to unity.

The relation between the meridional v_1 and normal v_3 displacements of an arbitrary point of the branched shell and displacements of a point of the coordinate surface u_1, u_3 has the form (Flügge, 1973)

$$v_1 = u_1 + x_3 \vartheta_1, \quad v_3 = u_3 \tag{16}$$

where

$$\vartheta_1 = k_1 u_1 - u_3' \tag{17}$$

Here, ϑ_1 is the angle of rotation of the normal to the coordinate surface in the direction x_1; $(\dots)' = \frac{d(\dots)}{dx_1}$; k_1 is the principal curvature of the coordinate surface in the direction x_1, $k_1 = \theta'$; and $\pi - \theta$ is the angle between the normal to the coordinate surface and the axis z. The strain components ε_{11}, ε_{22} at an arbitrary point of the shell are related to the strains ε_1, ε_2 and the changes of curvatures κ_1, κ_2 of its coordinate (middle) surface in the form ($\varepsilon_{12} = 0$ due to symmetry and $\varepsilon_{13} = \varepsilon_{23} = \varepsilon_{33} \approx 0$ according to the Kirchoff–Love assumptions)

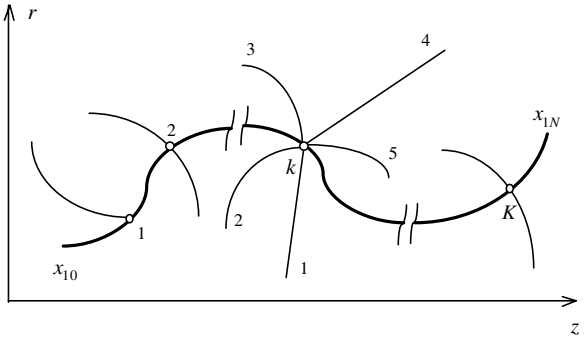

Fig. 5. The branched meridian of a shell (thick line is the meridian of a basic shell, thin lines are meridians of branches, and the branch nodes are shown by white circles and numbered from one up to K).

$$\varepsilon_{11} = \varepsilon_1 + x_3\kappa_1 \ (1,2) \tag{18}$$

where

$$\varepsilon_1 = u_1' + k_1 u_3, \ \varepsilon_2 = \rho u_1 + k_2 u_3, \ \kappa_1 = \vartheta_1', \ \kappa_2 = \rho\vartheta_1 \tag{19}$$

Here, k_2 is the principal curvature of the coordinate surface in the circumferential direction, $k_2 = \frac{\sin\theta}{r}$; $\rho = \frac{\cos\theta}{r}$, and the symbol (1,2) implies that the new equation follows from the equation under consideration by the cyclic substitution of the subscripts 1 and 2.

The equations of equilibrium (Flügge, 1973) are given by

$$\begin{aligned} &(rN_1)' - r\rho N_2 + rk_1 Q_1 + rq_1 = 0 \\ &(rQ_1)' - rk_1 N_1 - rk_2 N_2 + rq_3 = 0 \\ &(rM_1)' - r\rho M_2 - rQ_1 = 0 \end{aligned} \tag{20}$$

where N_1 and Q_1 are the normal and transverse shear forces acting in the cross section $x_1 = \text{const}$; N_2 is the normal force acting in the cross section $x_2 = \text{const}$; M_1 and M_2 are meridional and circumferential bending moments; and q_1, q_3 are the distributed loads referred to the coordinate surface.

One assumes the initial isotropy for the material of the branched shell, no effect of the damage on the elastic deformation of the shell, and different behaviors in tension and compression for the material of the branched shell under creep and creep damage conditions. Assuming also that total strains are composed of an elastic part, thermal part and a part due to creep, and using the generalized Hooke's law, one obtains

$$\sigma_{11} = \frac{E}{1-\nu^2}(\varepsilon_{11} + \nu\varepsilon_{22}) - \sigma_{11}^a \ (1,2) \tag{21}$$

where the additional terms related to the thermal gradients and creep are expressed as

$$\sigma_{11}^a = \frac{E}{1-\nu^2}[(1+\nu)\alpha_T(T - T_0) + p_{11} + \nu p_{22}] \ (1,2) \tag{22}$$

Here, E, ν and α_T are the Young's modulus, Poisson's ratio and the coefficient of linear thermal expansion, respectively. The creep strains in Eq. (22) are defined by Eqs. (7) and (8) describing creep deformation and creep damage growth in the material of the branched shell with different behavior in tension and compression.

One now introduces the membrane forces and the bending moments

$$\begin{aligned} N_1 &= \int_{-h/2}^{h/2} \sigma_{11} \mathrm{d}x_3 \ (1,2) \\ M_1 &= \int_{-h/2}^{h/2} \sigma_{11} z \mathrm{d}x_3 \end{aligned} \tag{23}$$

Substituting the values of ε_{11}, ε_{22} from Eq. (18) in Eq. (21) and the resulting expressions for the stresses σ_{11}, σ_{22} in Eq. (23) and integrating over the shell thickness, one obtains the physical equations of shell theory as follows:

$$\begin{aligned} N_1 &= C_{00}\varepsilon_1 + C_{01}\varepsilon_2 + C_{10}\kappa_1 + C_{11}\kappa_2 - N_1^a \\ N_2 &= C_{01}\varepsilon_1 + C_{00}\varepsilon_2 + C_{11}\kappa_1 + C_{10}\kappa_2 - N_2^a \\ M_1 &= C_{10}\varepsilon_1 + C_{11}\varepsilon_2 + C_{20}\kappa_1 + C_{21}\kappa_2 - M_1^a \\ M_2 &= C_{11}\varepsilon_1 + C_{10}\varepsilon_2 + C_{21}\kappa_1 + C_{20}\kappa_2 - M_2^a \end{aligned} \tag{24}$$

where C_{pq} are the stiffness characteristics of the shell

$$C_{pq} = \int_{-\frac{h}{2}}^{\frac{h}{2}} \frac{E\nu^q}{1-\nu^2} x_3^p \mathrm{d}x_3 \quad (p = 0,1,2; \ q = 0,1) \tag{25}$$

N_i^a, M_i^a $(i = 1,2)$ are the additional terms related to the thermal gradients and creep

$$N_1^a = \int_{-\frac{h}{2}}^{\frac{h}{2}} \sigma_{11}^a \mathrm{d}x_3, \; M_1^a = \int_{-\frac{h}{2}}^{\frac{h}{2}} \sigma_{11}^a x_3 \mathrm{d}x_3 \; (1,2) \tag{26}$$

If elastic constants do not vary in the direction x_3, for example, with changing of the temperature, the integrals in Eq. (25) can then be calculated analytically as $C_{10} = C_{11} = 0$, $C_{00} = Eh/(1-\nu^2)$, $C_{01} = \nu C_{00}$, $C_{20} = C_{00}h^2/12$, $C_{21} = \nu C_{20}$, but Eq. (26) can be integrated only numerically.

Thus, the kinematic equations (17) and (19), static equations (20) and physical ones (24) form a complete system of the basic equations describing the creep deformation and creep damage at each instant of time in the shell with the basic meridian and in each branch made from materials with different behavior in tension and compression.

4. Initial/boundary-value problem

One now shows how it is possible to reduce the creep problem for a branched shell to the numerical integration at each time instant of the differential equations describing the creep deformation of each branch and of the basic shell. For this purpose, one introduces the radial N_r and axial N_z components of the forces acting in the cross section $x_1 = \text{const}$ of the branched shell as well as the corresponding components of the displacement of the coordinate surface as follows:

$$N_r = N_1 \cos\theta + Q_1 \sin\theta, \quad N_z = N_1 \sin\theta - Q_1 \cos\theta \quad u_r = u_1 \cos\theta + u_3 \sin\theta,$$
$$u_z = u_1 \sin\theta - u_3 \cos\theta \tag{27}$$

In the same way one writes also similar equalities for the radial and axial components of the surface loads

$$q_r = q_1 \cos\theta + q_3 \sin\theta, \quad q_z = q_1 \sin\theta - q_3 \cos\theta \tag{28}$$

One now introduces a vector of resolving functions

$$\mathbf{Y} = \{\mathbf{N}, \mathbf{U}\}^{\mathrm{T}}, \quad \mathbf{N} = \{N_r, N_z, M_1\}^{\mathrm{T}}, \quad \mathbf{U} = \{u_r, u_z, \vartheta_1\}^{\mathrm{T}} \tag{29}$$

Basic Eqs. (17), (19), (20) and (24) of the shell theory can then be transformed to the following system of nonlinear differential equations presented in vector form

$$\mathbf{Y}' = [\mathbf{P}]\mathbf{Y} + \mathbf{f} \tag{30}$$

Here the matrix of the system $[\mathbf{P}]$ and the free-term vector $\mathbf{f}$ have the following non-zero components:

$$P_{11} = -\rho(1+\lambda_1); \quad P_{12} = -P_{54} = -\lambda_1 k_2; \quad P_{13} = -P_{64} = \frac{\lambda_2}{r};$$
$$P_{14} = \frac{1}{r^2}(C_{02} + C_{01}\lambda_1 - C_{11}\lambda_2); \quad P_{16} = P_{34} = \frac{\rho}{r}(C_{12} + C_{11}\lambda_1 - C_{21}\lambda_2); \quad P_{22} = -\rho;$$
$$P_{31} = -P_{46} \quad = \sin\theta + \lambda_3 \rho \cos\theta; \quad P_{32} = -P_{56} = (\lambda_3 k_2 - 1)\cos\theta; \quad P_{33} = \rho(\lambda_4 - 1);$$
$$P_{36} = \rho^2(C_{22} - C_{11}\lambda_3 - C_{21}\lambda_4); \quad P_{41} = \frac{C_{20}}{\delta}\cos^2\theta; \quad P_{42} = P_{51} = \frac{C_{20}}{\delta}\sin\theta\cos\theta;$$
$$P_{43} = P_{61} \quad = -\frac{C_{10}}{\delta}\cos\theta; \quad P_{44} = \rho\lambda_1; \quad P_{52} = \frac{C_{20}}{\delta}\sin^2\theta; \quad P_{53} = P_{62} = -\frac{C_{10}}{\delta}\sin\theta; \quad P_{63} = \frac{C_{00}}{\delta};$$
$$P_{66} = -\rho\lambda_4; \quad f_1 = \frac{1}{r}(-\lambda_1 N_1^a - N_2^a + \lambda_2 M_1^a) - q_r; \quad f_2 = -q_z; \quad f_3 = \rho(\lambda_3 N_1^a + \lambda_4 M_1^a - M_2^a);$$
$$f_4 = \frac{\cos\theta}{\delta}(C_{20}N_1^a - C_{10}M_1^a); \quad f_5 = \frac{\sin\theta}{\delta}(C_{20}N_1^a - C_{10}M_1^a); \quad f_6 = \frac{1}{\delta}(C_{00}M_1^a - C_{10}N_1^a) \tag{31}$$

where

$$\lambda_1 = \frac{1}{\delta}(C_{11}C_{10} - C_{01}C_{20}); \quad \lambda_2 = \frac{1}{\delta}(C_{11}C_{00} - C_{10}C_{01}); \quad \lambda_3 = \frac{1}{\delta}(C_{20}C_{11} - C_{21}C_{10});$$
$$\lambda_4 = \frac{1}{\delta}(C_{21}C_{00} - C_{11}C_{10}); \quad \delta = C_{00}C_{20} - C_{10}^2 \tag{32}$$

The surface loads as well as the effects of thermal gradient and creep are included at the free-term vector **f** .

The system of non-linear differential Eq. (30) must be complemented by the boundary conditions at the non-node ends of the branched shell

$$[\mathbf{D}]\mathbf{Y} = \mathbf{d} \tag{33}$$

and by kinematic

$$\mathbf{U}_+ = \mathbf{U}_- = \mathbf{U}_p \quad (p = 1, 2, \ldots, M_p) \tag{34}$$

and static matching conditions at the branch nodes

$$\mathbf{N}_+ = \mathbf{N}_- + \sum_{p=1}^{M_k} \mathbf{N}_p \tag{35}$$

where the specific form of the rectangular matrix [**D**] and the vector **d** depends on the kind of the boundary conditions used. This will be discussed in the next section of the paper for various modes of fixing the shell; the subscripts '+' and '−' correspond to the limiting values of the vector-functions **N** and **U** for the basic shell at the kth node from the left and the right, respectively; and the subscript $p = 1, 2 \ldots, M_p$ corresponds to the values of the vector-functions **N** and **U** for each pth branch at the kth node. It is clear now that the selection of the resolving functions in the form (27) allows the conditions at the branch nodes to be formulated in the simplest way.

Thus, the analysis of the creep deformation and creep damage at each instant of time in the axisymmetrically loaded branched shell made from materials with different behavior in tension and compression reduces to a non-linear one-dimensional boundary-value problem given by Eqs. (30), (33), (34) and (35) with time as a parameter. Due to the time dependence of the components of the vector **f** related to the creep, this formulated boundary-value problem must be considered simultaneously with the initial-value problem (with respect to time) for the ordinary differential Eqs. (7) and (8) with the natural initial conditions $p_{11} = p_{22} = \varphi = 0$ at $t = 0$. Thus, the proposed approach based on the direct integration of the initial-value problem for Eqs. (7) and (8) by one of the numerical methods involves reducing the non-linear boundary-value problem to the solution of a sequence of linear boundary value problems with known components of the vector **f** related to the creep. The integration of the initial-value problem for Eqs. (7) and (8) will be discussed later in this section. Each linearized boundary-value problem (with fixed components of the vector **f**) will be solved by the discrete orthogonal shooting method of Godunov (1961) reducing it to a series of Cauchy problems which will be integrated by the Runge–Kutta's method with the Gram–Schmidt's discrete orthogonalization. The advantages of the discrete orthogonal shooting method of Godunov are discussed in detail, for example, in the monograph by Grigolyuk and Shalashilin (1991).

For an arbitrary branch, the general solution of Eq. (30) under the assumption that one knows the creep terms in the vector**f** at each instant time takes the form

$$\mathbf{Y} = [\tilde{\mathbf{Y}}]\mathbf{C} + \overline{\mathbf{Y}} \tag{36}$$

where $[\tilde{\mathbf{Y}}]$ is a matrix whose columns are solutions of the Cauchy problems for the homogeneous system of Eq. (30) satisfying the homogeneous boundary conditions (33) at $x = x_0$ resulting from Eq. (33) with $\mathbf{d} = 0$, $[\tilde{\mathbf{Y}}] = \begin{bmatrix} [\tilde{\mathbf{N}}] \\ [\tilde{\mathbf{U}}] \end{bmatrix}$; $\overline{\mathbf{Y}}$ is the vector consisting at each instant in time the solution of the Cauchy problem for the inhomogeneous system of Eq. (30) satisfying the inhomogeneous boundary conditions (33) at $x = x_0$, $\overline{\mathbf{Y}} = \{\overline{\mathbf{N}}, \overline{\mathbf{U}}\}$;

and **C** is the vector for the integration constants. Using Eq. (34) one can express the vector for the integration constants for the pth branch at the node in the form

$$\mathbf{C}_p = [\tilde{\mathbf{U}}]_p^{-1}[\tilde{\mathbf{U}}]_-\mathbf{C}_- + [\tilde{\mathbf{U}}]_p^{-1}(\overline{\mathbf{U}}_- - \overline{\mathbf{U}}_\mathbf{p}) \tag{37}$$

Then using Eq. (35) one obtains the following equations for reconstructing the particular solutions for a basic shell with a transition over the kth branch node

$$[\tilde{\mathbf{N}}]_+ = [\tilde{\mathbf{N}}]_- + \sum_{p=1}^{M_k} [\tilde{\mathbf{N}}]_p [\tilde{\mathbf{U}}]_p^{-1} [\tilde{\mathbf{U}}]_-$$
$$\overline{\mathbf{N}}_+ = \overline{\mathbf{N}}_- + \sum_{\mathbf{p=1}}^{\mathbf{M_k}} (\overline{\mathbf{N}}_\mathbf{p} + [\tilde{\mathbf{N}}]_\mathbf{p} [\tilde{\mathbf{U}}]_\mathbf{p}^{-1} (\overline{\mathbf{U}}_- - \overline{\mathbf{U}}_\mathbf{p})) \tag{38}$$

In addition, it is necessary to note that

$$[\tilde{\mathbf{U}}]_+ = [\tilde{\mathbf{U}}]_-, \ \overline{\mathbf{U}}_+ = \overline{\mathbf{U}}_- \tag{39}$$

These relations follow from the kinematic condition of conjugation at the branch nodes (34). The obtained quantities $[\tilde{\mathbf{N}}]_+$, $[\tilde{\mathbf{U}}]_+$, $\overline{\mathbf{N}}_+$ and $\overline{\mathbf{U}}_+$ are needed for finding at each time instant the solution given by Eq. (36) in the interval between the kth and $(k+1)$th nodes.

Returning to the integration of the initial-value problem for Eqs. (7) and (8), it is possible to use various numerical time integration algorithms (Bathe, 1996; Bellenger and Bussy, 2001; Boyle and Spence, 1983; Hayhurst et al., 1975; Hyde et al., 1996; Kraus, 1980; Lemaitre and Chaboche, 1990; Murakami and Liu, 1995; Murakami et al., 2000; Saanouni et al., 1986; Simo and Hughes, 1998). The application of the well known and simple time discretization method by step to step (Rabotnov, 1969) related to the integration of Eqs. (7) and (8) by the Euler's method with explicit scheme will lead to the large reduction of step sizes and may lead to an unstable solution due to the acceleration of creep deformation in the tertiary creep stage and due to the rapid growth of creep damage since the resulting equations are highly non-linear and stiff in nature (Chen and Hsu, 1988; Kumar et al., 1980). Constant step time algorithms based on the explicit methods are only conditionally stable, that is, the numerical solution is stable if the constant time step value is sufficiently small, but it is unstable if the time step is larger than some critical value. Therefore, time integration algorithms based on the explicit Euler method with automatic time step control (Kumar et al., 1980) or on the implicit backward Euler method (Chaboche and Cailletaud, 1996; Saleeb et al., 2001) have been recommended with detailed numerical treatments to use in the creep analysis of structures, but numerical examples with tertiary creep stage and creep damage growth have been not considered in these analysis. On the other hand, a high-order time integration method should be more efficient than a low-order method in creep damage analysis. For example, the truncation error of one time step of the Euler's method is, for small time step Δt, can be defined as $C_e \Delta t$ while the classic Runge–Kutta method has an error $C_{rk} \Delta t^4$, where C_e and C_{rk} are constants. Then, to achieve an error smaller than a certain specified value δ, Euler's method has to use a time step size not larger than δ / C_e. Thus, the classic Runge–Kutta method may use a time step of $(\delta / C_{rk})^{1/4}$ which is much larger than the time step size of Euler's method, when δ is sufficiently small. For example, the cost of the calculations in the creep damage applications by the implicit backward Euler method is twice as high as the cost of calculations by the explicit Runge–Kutta–Merson's method with automatic time step control (Ling et al., 2000). Thus, the time integration algorithm with an implicit backward Euler method used in the creep analysis of shells by Altenbach and Naumenko (1997), Providakis (2002), and Shariyat and Eslami (1996) is computationally expensive. Furthermore, the varying time step algorithm based on the Runge–Kutta–Merson's method is much faster than its constant time step version, because it does not need small time steps and it concentrates its computational effort only on those time intervals that are needed, taking large strides over intervals. Also, a varying time step algorithm ensures that numerical instability does not occur. Taking into account all these arguments, the fourth-order Runge–Kutta–Merson's method with automatic selection of time step sizes will be used in order to solve the initial value problem for Eqs. (7) and (8). This time integration scheme has been applied for the first time in the study of creep of structures, to the authors' best knowledge, by Zolochevsky (1980, 1982) for the numerical analysis of creep deformation and creep damage growth in thin-walled shells with non-branched meridian. It has been later used in creep analysis by many authors, for example, by Hayhurst et al. (1984), Altenbach and Zolochevsky (1991), Sichov (1998), and Ling et al. (2000). Let us introduce the following vector function including the creep strains and damage variable in all discretization points of the branched shell

$$\mathbf{G} = \{p_{11}, p_{22}, \varphi\}^{\mathrm{T}} \tag{40}$$

Eqs. (7) and (8) can then be represented in vector form as follows

$$\frac{d\mathbf{G}}{dt} = \mathbf{F}[t, \mathbf{G}(t)] \tag{41}$$

Here, $\mathbf{F}[t,\mathbf{G}(t)]$ is a non-linear vector function defined by the right-hand sides of Eqs. (7) and (8) complemented by Eqs. (21), (22) and (18). Then according to the fourth-order Runge–Kutta–Merson's method, the unknown functions at each point of the shell for the next instant time $t+\Delta t$ can be calculated as:

$$G_k(t+\Delta t) = G_k(t) + 0.5(r_1^k + 4r_4^k + r_5^k) + 0(\Delta t^5) \tag{42}$$

where

$$r_1^k = \frac{\Delta t}{3} F_k[t, G_j(t)], \quad r_2^k = \frac{\Delta t}{3} F_k\left[t + \frac{\Delta t}{3}, G_j(t) + r_1^j\right], \quad r_3^k = \frac{\Delta t}{3} F_k\left[t + \frac{\Delta t}{3}, G_j(t) + \frac{1}{2}(r_1^j + r_2^j)\right],$$
$$r_4^k = \frac{\Delta t}{3} F_k\left[t + \frac{\Delta t}{2}, G_j(t) + \frac{3}{8}(r_1^j + 3r_3^j)\right], \quad r_5^k = \frac{\Delta t}{3} F_k\left[t + \Delta t, G_j(t) + \frac{3}{2}(r_1^j - 3r_3^j + 4r_4^j)\right] \tag{43}$$

This method of the time integration allows for the estimation of the absolute error be of the order of Δt to the fifth power. The initial time step size $\Delta t = \Delta t_0$ is assigned, and its subsequent values can be chosen automatically on the basis of the condition that the cumulative absolute error in the calculations

$$\varepsilon = \max_k \left(r_1^k - \frac{9}{2} r_3^k + 4r_4^k - \frac{1}{2} r_5^k \right) \tag{44}$$

does not exceed a certain specified value δ. Here the following criterion for the change in the step size has been used. If $\varepsilon > \delta$, then the step Δt decreases by a factor of two and the calculations are repeated. If $\varepsilon < \frac{\delta}{32}$, then the time step is doubled and the calculations are continued. Otherwise, the step size remains as the previous one. Note also that calculations of the right sides in Eq. (43) requires the fivefold solution of the linear boundary-value problem with fixed components of creep strain in Eq. (30) at each time step. Thus, in the incremental approach considered here, the non-linear creep analysis is replaced by a series of linear analyses for progressively increasing time, after each of which the material creep features in the shell are recomputed. Furthermore, accurate time integration is provided until $t \leqslant t_{\max}$ or $\varphi \leqslant \varphi_*$. Finally, note that the presented approach can be considered as a particular form of the method of the continuation of the solution with respect to a parameter, discussed, for example, in the monograph by Grigolyuk and Shalashilin (1991).

5. Numerical examples

5.1. Example 1: primary creep behavior of a cylindrical shell

To test the proposed model for numerical analysis of the creep deformation of thin shells, one compares its predictions against the numerical results by Takezono and Fujioka (1981) for the primary creep behavior of the cylindrical shell subjected to internal pressure $q_3 = 1.47$ MPa at the temperature of $T = T_0 = 808.15$ K. These authors used the implicit Euler's method in the time-integration procedure and the finite difference method to find solutions for the linearized boundary-value problems.

The geometrical parameters of the cylindrical shell are: $r = 0.4$ m, $\theta = \frac{\pi}{2}$, $k_1 = 0$. The length of the shell and the thickness are: $2L = 0.4$ m and $h = 0.004$ m, respectively. Both ends of the shell are simply supported. Taking into account the symmetry of the shell, one considers one half of the shell with such boundary conditions as: $N_r = u_z = \vartheta_1 = 0$ for $x_1 = 0$ and $N_z = M_1 = u_r = 0$ for $x_1 = L$. The material of the shell is stainless steel SUS 22 with elastic constants $E = 1.3 \times 1\ 0^5$ MPa and $v = 0.3$. Only the primary creep behavior of steel will be considered, without consideration of the creep damage growth. Creep characteristics of the material are independent from the kind of loading, and relations (13) take place. Material constants in Eq. (9) are: $K_+ = 1.41 \times 1\ 10^3\ \text{GPa}^{-m-\beta}\ \text{h}^{-1}$, $m = 10.3$, $\beta = 0.661$, $q = 0$.

Calculations have been performed using Eqs. (15) and (14) with the initial value of the time step $\Delta t_0 = 10^{-8}$ h and with accuracy $\delta = 10^{-11}$ until $t_{\max} = 5$ h. Numerical results have been obtained for discretization with 60 points along the meridian and 20 points along the thickness of the shell.

Fig. 6 shows a satisfactory agreement at the time instant $t = 5$ h between the results generated from the proposed approach (—) and the results by Takezono and Fujioka (1981) (•••).

5.2. Example 2: creep deformation and creep damage in a cylindrical shell for a material with different behavior in tension and compression

One analyzes the effect of the tension–compression asymmetry of the material on the creep deformation and the patterns of creep damage evolution in a cylindrical shell subjected to external pressure $q_3 = -5$ MPa. The geometrical parameters of the shell have the following values: $r = 0.2$ m, $\theta = \frac{\pi}{2}$, $k_1 = 0$, $h = 0.01$ m, the length $L = 0.2$ m. One edge of the shell is fixed ($u_r = u_z = \vartheta_1 = 0$ for $x_1 = 0$), and the other is free ($N_r = N_z = M_1 = 0$ for $x_1 = L$). The material of the shell is an aluminum alloy AK4-1T at a temperature of $T = T_0 = 473$ K. The elastic constants are $E = 6 \times 10^4$ MPa, $\nu = 0.35$. The creep deformation and creep damage development in the material, as discussed earlier in Section 1, are strongly dependent on the kind of loading. Its creep curves up to creep rupture in uniaxial tension, uniaxial compression and pure torsion given in Fig. 4 can be described by Eqs. (9)–(11) with the critical value of the damage variable given by

$$\varphi_* = \sigma_i^2 (a - bI_1) \tag{45}$$

and with the following values of the material constants:

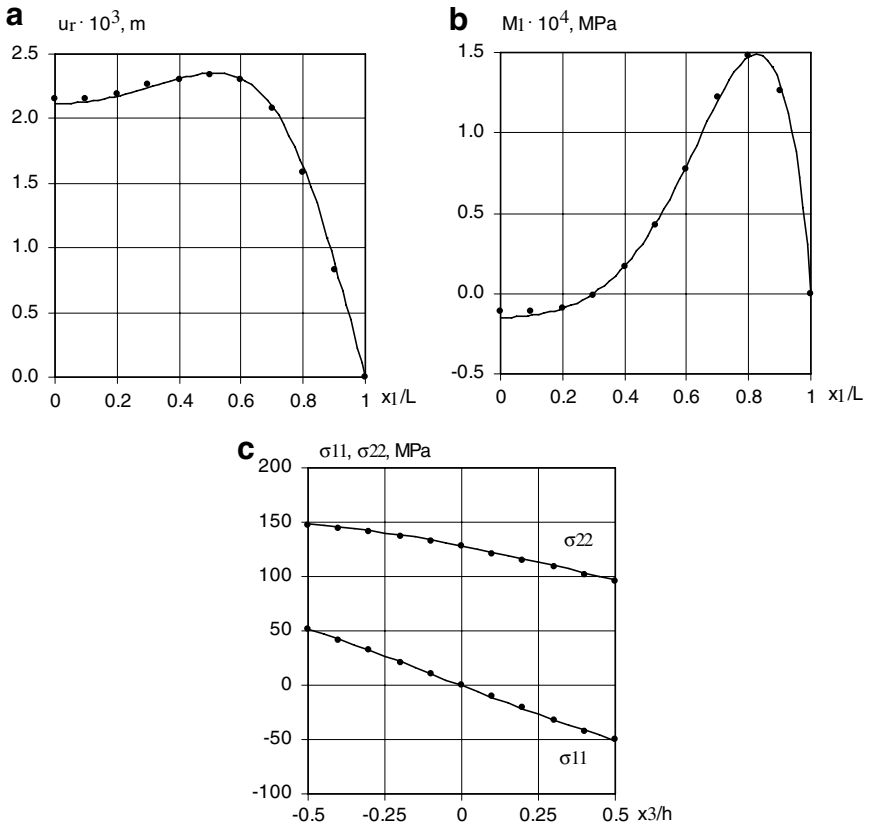

Fig. 6. Comparison of the present model predictions (—) with the results by Takezono and Fujioka (1981) (•••) at the time instant 5 h: variation of the radial displacement (a) and bending moment (b) along the meridian, and distribution of the meridional and circumferential stresses across a thickness at the cross section with $x_1 = 0.1756$ m (c).

$$K_+ = 55.0\ \text{GPa}^{-m}\ \text{h}^{-1}, \quad K_- = 22.5\ \text{GPa}^{-m}\ \text{h}^{-1}, \quad K_0 = 1.14 \times 10^4\ \text{GPa}^{-m}\ \text{h}^{-1},$$
$$m = 8,\ \beta = 0,\ q = 3 \tag{46}$$

where

$$a = 0.4\ \text{GPa}^{-1}, \quad b = 0.4\ \text{GPa}^{-2} \tag{47}$$

Numerical results have been obtained using Eqs. (7), (8), (12), (45), (46), (47) with the initial value of the time step $\Delta t_0 = 0.1$ h and with accuracy $\delta = 10^{-8}$ while $\varphi \leqslant 0.99\varphi_*$. Calculations are performed for discretization with 101 points along the meridian and 11 points along the thickness of the shell. The failure initiation time is found to be $t^* = 3.609 \times 10^4$ h, and the damage variable reaches its critical value on the outer surface of the free edge of the cylindrical shell.

For comparison the analogous numerical analysis of the creep deformation and creep damage development in the cylindrical shell is performed under the assumption of the same properties of the material in tension and compression. In this way numerical results have been obtained using Eqs. (15), (14), (13), (45) and (47) with the values of the material constants taken as:

$$K_+ = K_- = 55.0\ \text{GPa}^{-m}\ \text{h}^{-1}, \quad K_0 = 7.72 \times 10^3\ \text{GPa}^{-m}\ \text{h}^{-1}, \qquad m = 8,\ \beta = 0,\ q = 3 \tag{48}$$

under the conditions given by Eq. (47). It was established that the failure initiation time of the cylindrical shell is equal to $t^{**} = 1.038 \times 10^4$ h, and the damage variable reaches its critical value on the inner surface of the fixed edge of the cylindrical shell. Comparing the values t^* and t^{**}, it can be concluded that, in fact, the failure initiation time of the cylindrical shell made from the aluminum alloy AK4-1T with different properties in tension and compression is more than three times larger than the one with the same properties in tension and compression.

The results of the numerical analysis of the creep deformation and creep damage patterns in the cylindrical shell are given in Figs. 7–10. Here, the number 1 next to the curves refers to time t^* for the case of a shell made from the aluminum alloy AK4-1T with different properties in tension and compression, the number 2 refers to time t^{**} for the case of a shell from the material with identical properties in tension and compression, and the number 3 refers to the initial elastic solution.

In the case 1 the values of the creep damage variable on the outer surface and on the inner surface in the region near the fixed edge of a cylinder are different while the corresponding values in most regions of a cylinder are practically the same (Fig. 7a and b). It is seen (Fig. 7c) that the consideration of different behavior in tension and compression for the material leads to non-symmetrical damage distribution across the shell thickness in the fixed edge of the shell. Deflections and strains in the cylindrical shell (Fig. 8a–c) are essentially growing with time. By consideration of the same properties in tension and compression of the material a faster growth of damage variable, deflections and strains with time is observed.

The redistribution of stresses on the inner and outer surfaces of the cylindrical shell with time has a complex character, and it is essentially different in cases 1 and 2 (Fig. 9a–c). In general, there is a reduction in the initial maximum values, accompanied by a corresponding increase in the initial minimum values. Consideration of different behaviors of the material in tension and compression leads to the appearance of the stress in the middle surface of the cylindrical shell, movement of the neutral surface into the compressive field of the shell, and non-symmetrical stress distribution across the shell thickness (Fig. 9d).

Under the assumption of identical properties of the material in tension and compression, a significant relaxation takes place with time of the meridional stress on the inner surface of the cylindrical shell in its fixed edge (Fig. 10a). In contrast, this stress in a shell made from the aluminum alloy AK4-1T with different properties in tension and compression changes a little with time.

The meridional strain on the inner surface of the shell in its fixed edge in case 1 changes slower in comparison with case 2 (Fig. 10b). On the other hand, the growth of this strain in the free edge of the shell in case 1 is much more significant when compared with case 2 (Fig. 10c).

Thus, the numerical analysis has shown that in the case of taking into account different behavior of the shell material in tension and compression, the deflection growth, the change of the stress–strain state with time and damage evolution are essentially different from the approach based on the assumption of identical properties of the material in tension and compression.

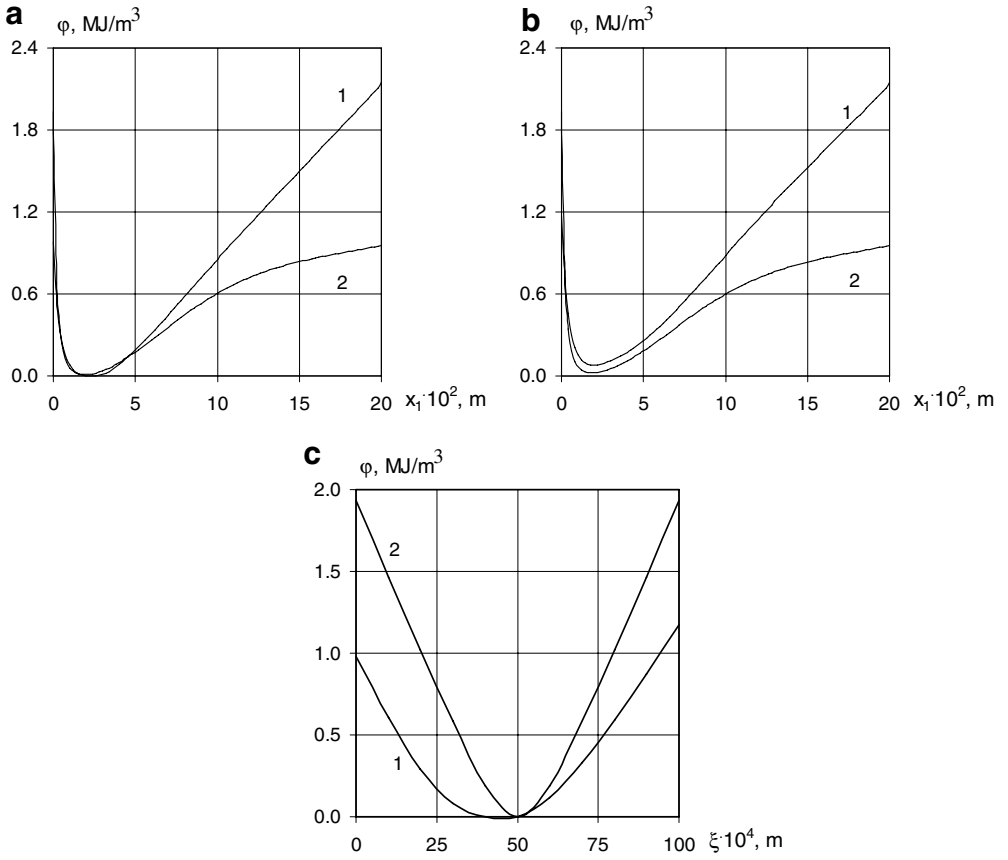

Fig. 7. Distribution of damage variable along the inner surface (a) and the outer surface (b), and its variation through the thickness of the cylindrical shell on the fixed edge (c), $\xi = x_3 + \frac{h}{2}$.

5.3. Example 3: creep deformation and creep damage in a branched shell for a material with different behavior in tension and compression

One analyzes here the effect of the tension–compression asymmetry of the material on the creep deformation and creep damage evolution in the branched shell (Fig. 11) at a temperature of $T = T_0 = 473$ K. The branch ABC consists of a cylinder AB and a circular toroidal segment BC, and the basic shell DCE consists of a conical part DC and a cylinder CE.

The characteristic dimensions are taken as follows: the length of sections $L_{AB} = L_{DC} = L_{CE} = L = 0.2$ m; the radius of the generating circle for a toroidal segment $R = \frac{2L}{\pi}$; and the radii of the coordinate surface $R_D = 0.2$ m, $R_C = R_E = 0.3$ m, $R_A = R_B = R_C + R$. The geometrical parameters of each section of the branched shell have the following values: $r = R_A$, $\theta = \frac{\pi}{2}$, $k_1 = 0$ for the section AB; $r = R_C + R \sin\theta$, $\theta = \frac{\pi}{2} + \frac{x_1 - x_{1B}}{R}$, $k_1 = R$ for the section BC, where x_{1B} is the value of coordinate x_1 at the point B; $r = R_D + x_1 \cos\theta$, $\cos\theta = \frac{R_C - R_D}{L_{DC}}$, $\sin\theta = \sqrt{1 - \cos^2\theta}$, $k_1 = 0$ for the section DC; and $r = R_C$, $\theta = \frac{\pi}{2}$, $k_1 = 0$ for the section CE.

The thickness h of the sections of the branch has the following values: $h = h_1 = 0.02$ m for the section AB; and for the section BC: if $x_{1B} \leqslant x_1 \leqslant x_{1C} - \Delta x_1$ then $h = h_1$, and if $x_{1C} - \Delta x_1 \leqslant x_1 \leqslant x_{1C}$ then $h = h_1 + (h_2 - h_1)\frac{x_1 - x_{1C} + \Delta x_1}{\Delta x_1}$, where $h_2 = 0.025$ m, $\Delta x_1 = 0.02$ m, x_1 is the meridional coordinate of the branch, x_{1B} and x_{1C} are the values of its meridional coordinate at the points B and C, respectively. For the sections of the basic shell the thickness is taken as follows: for the section DC: if $x_{1D} \leqslant x_1 \leqslant x_{1C} - \Delta x_1$ then $h = h_1$, and if $x_{1C} - \Delta x_1 \leqslant x_1 \leqslant x_{1C}$ then $h = h_1 + (h_2 - h_1)\frac{x_1 - x_{1C} + \Delta x_1}{\Delta x_1}$; for the section CE: if $x_{1C} \leqslant x_1 \leqslant x_{1C} + \Delta x_1$ then $h = h_2 + (h_1 - h_2)\frac{x_1 - x_{1C}}{\Delta x_1}$, and if $x_{1C} + \Delta x_1 \leqslant x_1 \leqslant x_{1E}$ then $h = h_1$, where x_1 is the meridional coordinate of

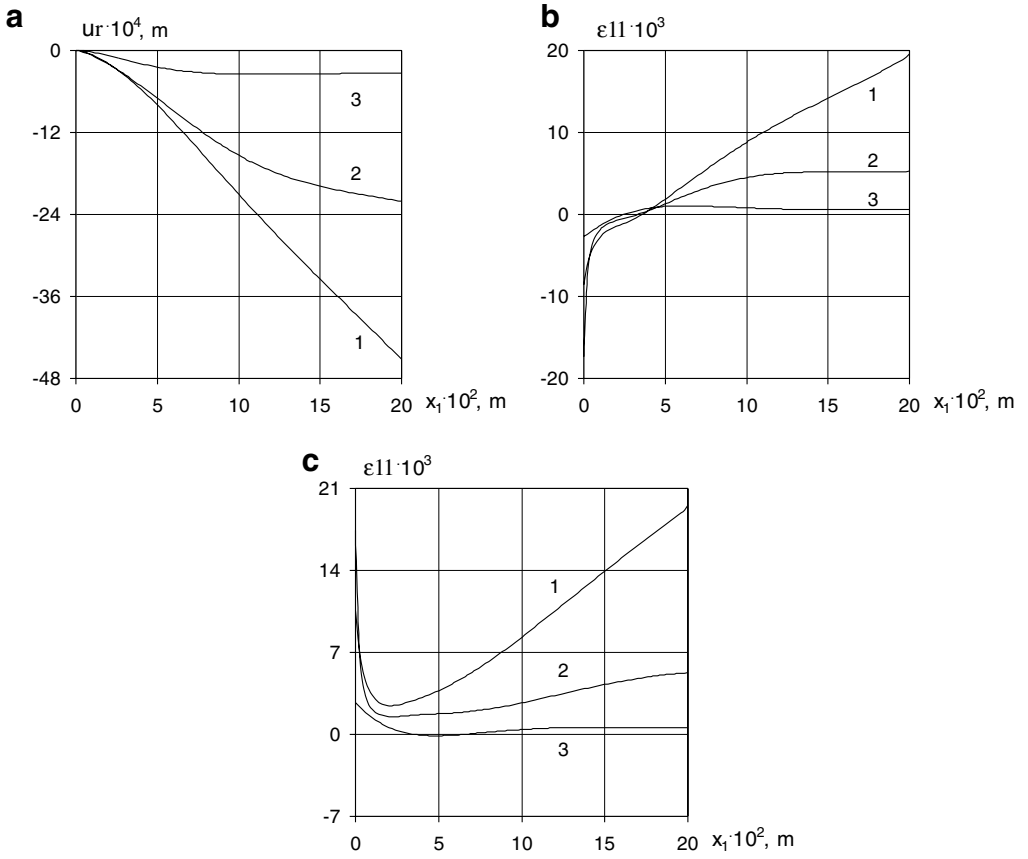

Fig. 8. Distribution of radial displacement along the meridian (a), and variation of meridional strain on the inner surface (b) and outer surface (c) of cylindrical shell.

the basic shell, x_{1D}, x_{1C} and x_{1E} are the values of its meridional coordinate at the points D, C and E, respectively.

The boundary condition at the point A of the branch is adopted to be the condition of symmetry ($N_r = u_z = \vartheta_1 = 0$ for $x_1 = x_{1A}$), and the boundary condition at the point E of the basic shell is adopted to be the condition of asymmetry ($N_z = u_r = \vartheta_1 = 0$ for $x_1 = x_{1E}$). The other non-node end of the basic shell with the applied compressive force N_z (Fig. 11) is free from the radial force and bending moment, and boundary conditions here can be written as $N_r = M_1 = 0$, $N_z = -0.05$ N/m for $x_1 = x_D$.

The surface load (Fig. 11) is equal to $q_3 = 5$ MPa. The material and its constants are the same as in the foregoing example.

Calculations have been performed with the initial value of the time step $\Delta t_0 = 0.01$ h and with accuracy $\delta = 10^{-9}$ while $\varphi \leqslant 0.99\varphi_*$. Numerical results are obtained for discretization with 121 points along the meridian of the basic shell and of the branch, and 11 points along the thickness of the branched shell. The results of creep deformation and creep damage accumulation have been obtained with and without tension–compression asymmetry of the material of the branched shell under consideration. In the case of the branched shell made from the aluminum alloy AK4-1T with different properties in tension and compression the failure initiation time is found to be $t^* = 6.316 \times 10^4$ h, and the damage variable reaches its critical value on the outer surface of the cylindrical shell CE near the branch node C at the point with the meridional coordinate $x_1 = 0.204$ m. On the other hand, in the case of the branched shell made from the material with identical properties in tension and compression the failure initiation time is found to be to $t^{**} = 3.221 \times 10^3$ h, and the damage variable reaches its critical value on the inner surface at the point C of the cylindrical shell. Thus, the assumption of the same properties of the material in tension and compression leads to the acceleration of

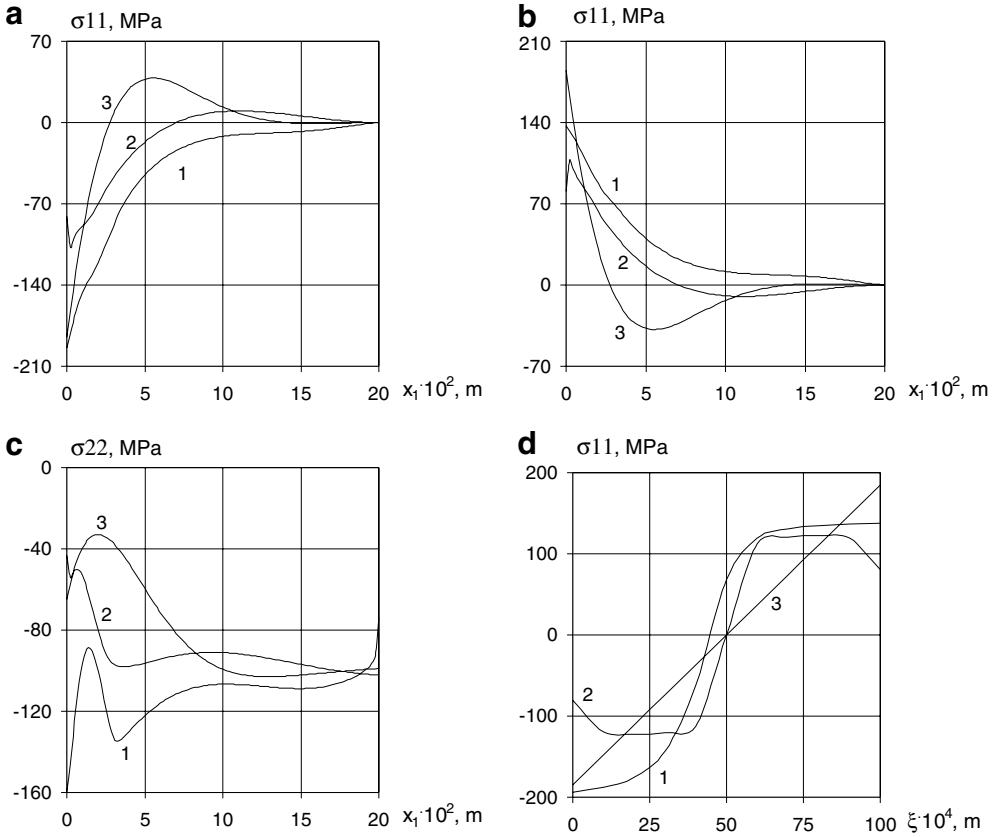

Fig. 9. Variation of the meridional stress on the inner surface (a) and outer surface (b), and circumferential stress on the inner surface (c), distribution of the meridional stress through the thickness of the fixed edge (d) of cylindrical shell, $\xi = x_3 + \frac{h}{2}$.

the creep damage growth and underestimation by a factor of about 20 of the failure initiation time. Furthermore, it is established that the effect of the tension–compression asymmetry of the material is more essential in the case of the branched shell in comparison to the previous example of the shell with non-branched meridian. Note that in order to understand the difference with the failure initiation time given above for the two numerical cases under consideration, namely different and same behavior under tension and compression, it is necessary to remember that the corresponding creep rupture times for tension and compression in basic experiments with the same absolute value of the stress, as it is seen from Fig. 4a and b, are different by a factor of about three.

Numerical analysis of the creep deformation and the creep damage development in the branched shell has shown a large difference between the equivalent stresses for the two cases under consideration that leads to a great difference between the failure initiation times.

The results of the numerical analysis of the creep deformation and creep damage development in the branched shell under consideration are shown in Figs. 12–15. Here, the meridional coordinate is determined as $x_1 \in [0, 0.4\text{ m}]$ for the basic shell as well as for branch including coordinate $x_1 \in [0, 0.2\text{ m}]$ for conical shell DC and cylinder AB, and $x_1 \in [0.2\text{ m}, 0.4\text{ m}]$ for cylinder CE and toroidal segment BC, respectively. The number 1 next to the curves in Figs. 12–15 refers to the time t^* for the case of a branched shell made from the aluminum alloy AK4-1T with different properties in tension and compression, the number 2 refers to the instant time t^{**} for the case of a branched shell from the material with the same behavior in tension and compression, and the number 3 refers to the initial elastic solution.

The plot for deflections of the branched shell under creep conditions and creep damage growth has a complex character (Fig. 12a and b). The maximum deflection is obtained at the point A of the cylindrical part of the branch. Even the displacements of the unloaded cylindrical part of the basic shell are significant due to its

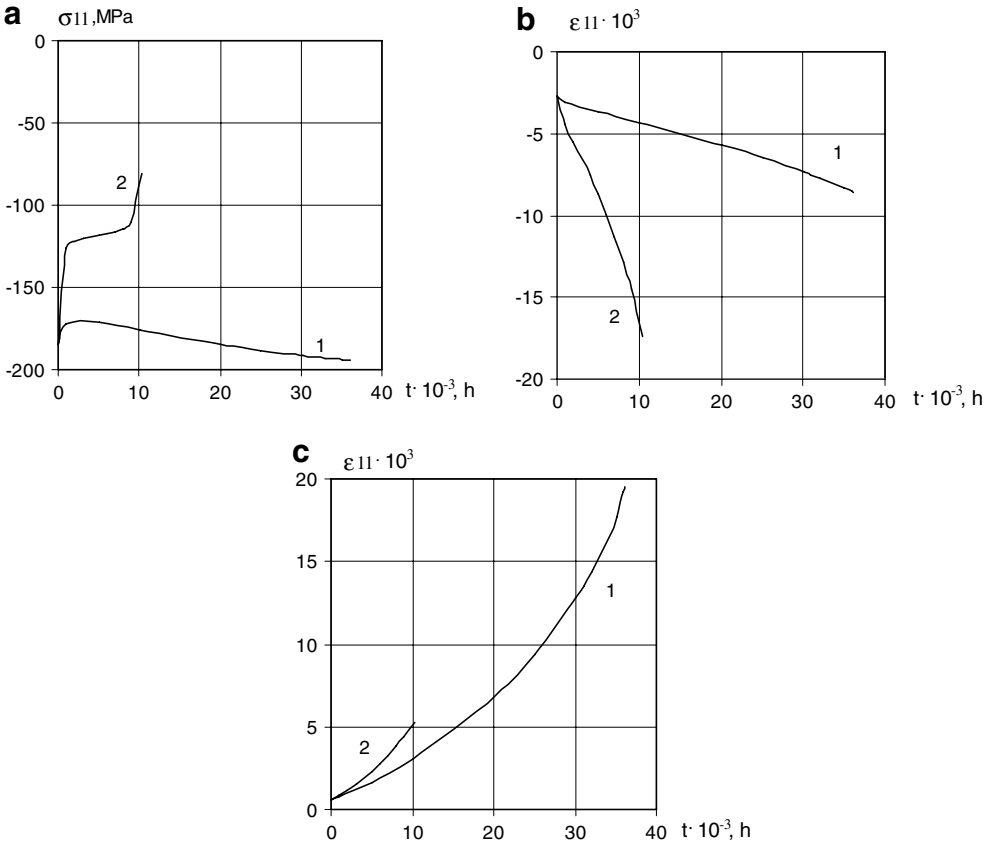

Fig. 10. Time variations on the inner surface of the cylindrical shell: (a) meridional stress in the fixed edge, (b) meridional strain in the fixed edge, (c) meridional strain in the free edge.

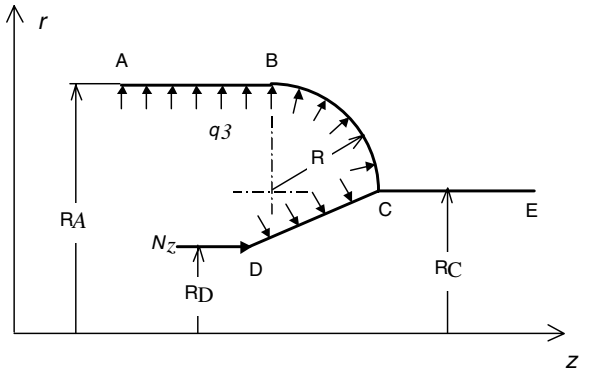

Fig. 11. Meridian of a branched shell of revolution (ABC-meridian of the branch, DCE-meridian of the basic shell).

connection with the other sections of the branched shell. The distribution of the meridional creep strain on the inner surface of the branched shell at the moment receding the failure initiation time is shown in Fig. 12c and d. There is a large difference between the displacements and creep strains in cases 1 and 2. However, the maximum absolute value of the creep strain is obtained at the point C of the unloaded cylindrical part of the basic shell, and this value is approximately the same in cases 1 and 2 (Fig. 12c and d). The last two statements apply also for the total strains (Fig. 13a and b). It is seen also that the contribution of the elastic strains to the deformation of the branched shell at the moment preceding the failure initiation time is very small; this deformation is mostly defined by the creep strains.

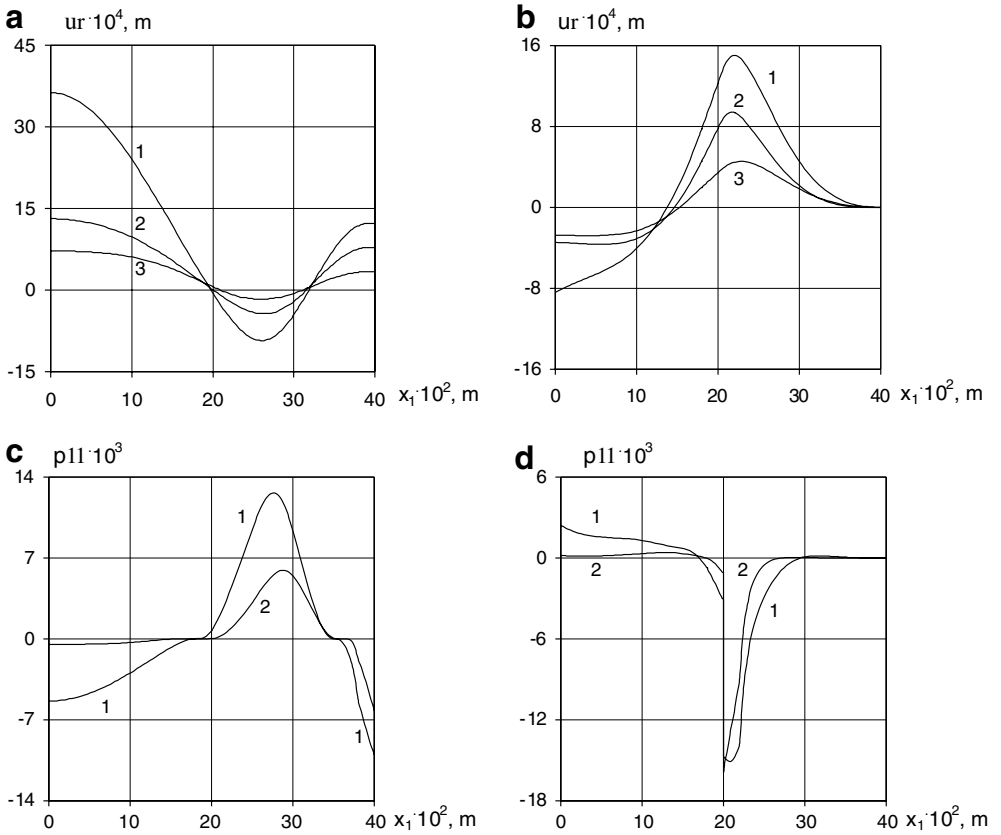

Fig. 12. Distribution of the radial displacement along the meridian of the branch (a) and basic shell (b), and variation of the meridional creep strain on the inner surface of the branch (c) and basic shell (d).

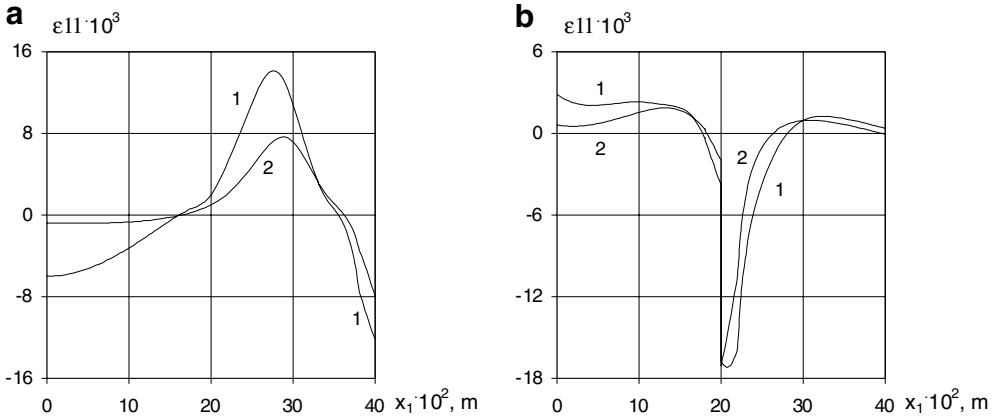

Fig. 13. Variation of the meridional total strain on the inner surface of the branch (a) and basic shell (b).

The final distribution of the creep damage variable on the inner surface of the branched shell is shown in Fig. 15a and b. The cylindrical part of the basic shell and toroidal segment of the branch are the most damaged sections of the branched shell under consideration. On the other hand, the damage in the conical part of the basic shell develops with time much slower. In the case of a branched shell made from the aluminum alloy AK4-1T with different properties in tension and compression, damage evolution is essentially different from that of a branched shell made from the material with identical behavior in tension and compression.

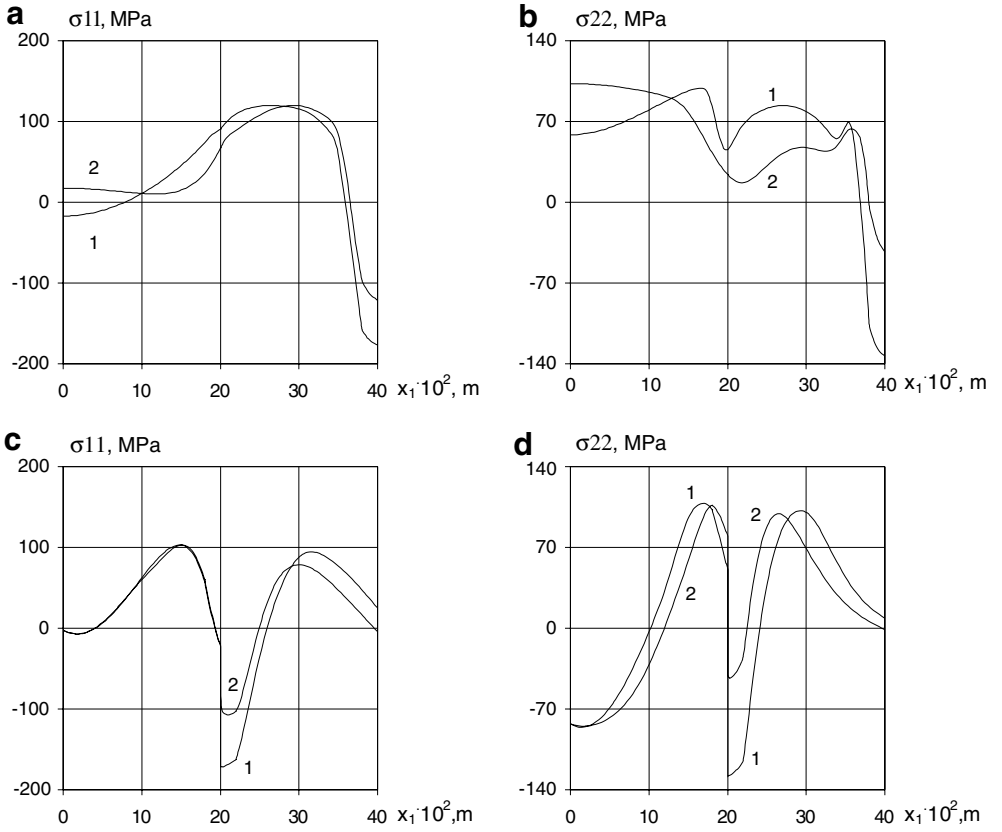

Fig. 14. Variation of the stresses on the inner surface of the branched shell for branch (a meridional stress, b circumferential stress) and for basic shell (c meridional stress, d circumferential stress).

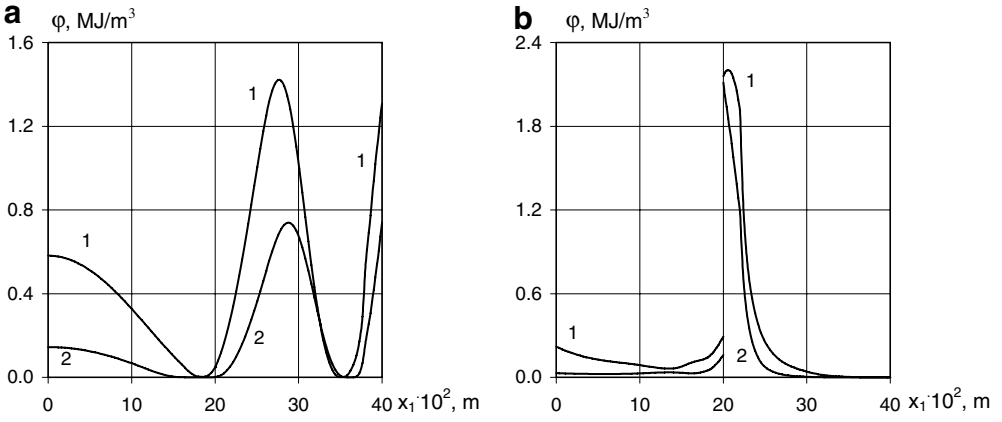

Fig. 15. Distribution of damage variable on the inner surface of the branch (a) and basic shell (b).

6. Discussion

In order to demonstrate the applicability of the proposed approach to the modeling of tertiary creep deformation and creep damage growth in thin-walled shells as well as to show the accuracy of the obtained numerical results, it is necessary to compare the creep damage patterns in the shell and its failure initiation time based on the present model with other numerical model predictions existing in the literature as well as with experimental data available for the shell.

For this purpose, first, one compares the proposed model predictions against the experimental results by Kaz (1955) for the tertiary creep of a closed-ended cylindrical shell at the temperature of $T = T_0 = 773$ K. The geometrical parameters of the shell have the following values: $r = 0.01802$ m, $\theta = \frac{\pi}{2}$, $k_1 = 0$, $h = 0.001982$ m, the length $2L = 0.07$ m. The shell is subjected to internal pressure $q_3 = 1.47$ MPa and to forces $N_z = \frac{q_3 r}{2}$ acting at the ends of the shell. Taking into account the symmetry of the shell, one considers one half of the shell with such boundary conditions as: $N_r = u_z = \vartheta_1 = 0$ for $x_1 = 0$ and $N_z = \frac{q_3 r}{2}$, $M_1 = u_r = 0$ for $x_1 = L$. The material of the shell is the carbon steel 20 with elastic constants $E = 1.56 \times 10^5$ MPa and $v = 0.3$. Creep and stress-rupture strength characteristics of the material depend on the kind of loading, and the creep deformation up to rupture can be described using the expression for the equivalent stress given by Eqs. (3) and (4) with the parameters $A = -\frac{1}{2}\alpha_1^2$, $B = \frac{3}{2}\alpha_1^2$, $\alpha C = \alpha_2$ by the following constitutive and damage evolution equations (Betten et al., 1999):

$$\begin{aligned} \dot{p}_{kl} &= B_1 \frac{\sigma_e^m}{(1-\omega)^p} t^{-\gamma} \left(\frac{3}{2} \alpha_1 \frac{s_{kl}}{\sigma_i} + \alpha_2 m_k m_l \right) \\ \dot{\omega} &= C_1 \frac{\sigma_e^Q}{(1-\omega^\vartheta)^q} t^{-\upsilon} \end{aligned} \tag{49}$$

based on the Rabotnov damage parameter ω. Material parameters in Eq. (49) are: $m = 6.742$, $\upsilon = 0$, $\vartheta = 1$, $\gamma = 0.2337$, $q = Q = 6.331$, $p = 4$, $\alpha_1 = 0.1$, $\alpha_2 = 1$, $B_1 = 1835$ GPa^{-m} h$^{\gamma-1}$ and $C_1 = 136.0$ GPa^{-Q} h$^{\upsilon-1}$. Calculations have been performed using Eq. (49) instead of Eqs. (7) and (8) with the initial value of the time step $\Delta t_0 = 0.1$ h and with accuracy $\delta = 10^{-4}$ while $\omega \leqslant 0.9$. Numerical results have been obtained for discretization with 60 points along the meridian and 11 points along the thickness of the shell. It was found that the failure initiation time obtained for the cylindrical shell under consideration in the present approach was equal to 1180 h compared with 1058 h in the experiments by Kaz (1955).

Second, one compares the proposed model predictions against the numerical results by Sichov (1998) for the tertiary creep of a cylindrical shell subjected to the internal pressure $q_3 = 32$ MPa at the temperature of $T = T_0 = 423$ K. The geometrical parameters of the shell have the following values: $r = 1$ m, $\theta = \frac{\pi}{2}$, $k_1 = 0$, $h = 0.2$ m, the length $L = 1$ m. The boundary condition at one edge of the shell is adopted to be the condition of symmetry ($N_r = u_z = \vartheta_1 = 0$ for $x_1 = 0$), and the other edge of the shell is fixed ($u_r = u_z = \vartheta_1 = 0$ for $x_1 = L$). The material of the shell is the aluminum alloy BS 1472 with elastic constants $E = 71.1$ GPa and $v = 0.3$. Creep and damage characteristics of the material are assumed to be independent from the kind of loading, and Eq. (49) has been used. Material parameters in Eq. (49) are: $m = p = 11.034$, $\upsilon = \gamma = 0.3099$, $q = 12.107$, $Q = 8.22$, $\alpha_1 = 1$, $\alpha_2 = 0$, $B_1 = 3.511 \times 10^{-31}$ MPa^{-m} h$^{\gamma-1}$ and $C_1 = 1.96 \times 10^{-23}$ MPa^{-Q} h$^{\upsilon-1}$. It is clear that the shell under consideration is a shell of the middle thickness, however the Kirchoff–Love assumptions have been accepted in the proposed approach as well as by Sichov (1998). These assumptions were made in the present investigation only for the sake of comparison with the numerical results by Sichov (1998). Calculations have been performed using Eq. (49) instead of Eqs. (7) and (8) with the initial value of the time step $\Delta t_0 = 1$ h and with accuracy $\delta = 10^{-3}$ while $\omega \leqslant 0.35$. Numerical results have been obtained for discretization with 201 points along the meridian and 17 points along the thickness of the shell.

Fig. 16 shows a satisfactory agreement on the inner surface of the fixed edge of the shell between the results generated from the proposed approach (—) and the results by Sichov (1998) (•••).

Third, one compares our model predictions against the numerical results by Sichov (2003) for the tertiary creep of a circular plate subjected to the pressure $q_3 = 0.3$ MPa at the temperature of $T = T_0 = 573$ K. The inner and outer radii of the circular plate are $R_0 = 0.01$ m and R_n=0.04 m, respectively, and the thickness $h = 0.003$ m. The circular plate can be considered as a particular case of the shell of the revolution with the following values of the geometrical parameters: $r = R_0 + x_1$, $\theta = 0$, $k_1 = 0$. One edge of the plate is free ($N_r = N_z = M_1 = 0$ for $x_1 = 0$), and the other is fixed, but with possible movement in the radial direction ($N_r = u_z = \vartheta_1 = 0$ for $x_1 = R_n - R_0$). The material of the plate is the aluminum alloy D16AT with elastic constants $E = 65$ GPa and $v = 0.3$. Creep and damage characteristics of the material are assumed to be independent from the kind of loading, and Eq. (49) has been used. Material parameters in Eq. (49) are: $m = p = Q = q = 3$, $\gamma = \upsilon = 0$, $\vartheta = 1.4$, $\alpha_1 = 1$, $\alpha_2 = 0$, $B_1 = 0.335 \times 10^{-7}$ MPa^{-m} h$^{\gamma-1}$ and $C_1 = 1.9 \times 10^{-7}$ MPa^{-Q} h$^{\upsilon-1}$. Calculations have been performed using Eq. (49) instead of Eqs. (7) and (8) with

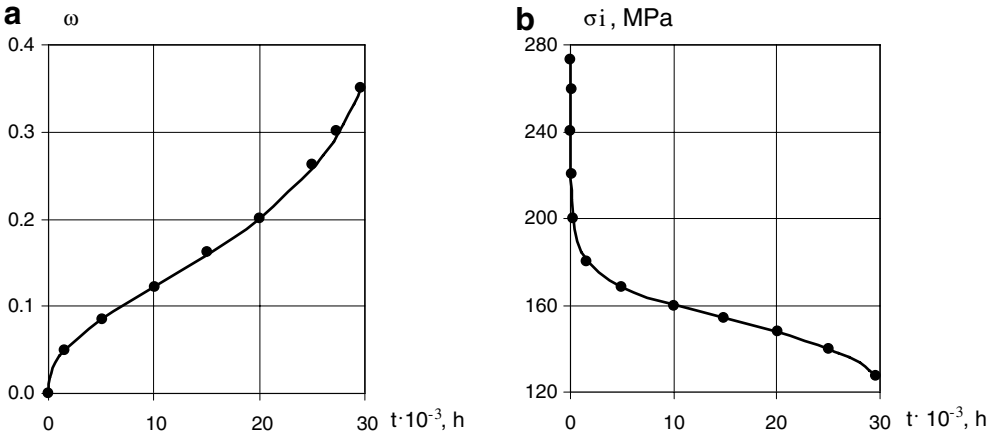

Fig. 16. Comparison of the present model predictions (—) with the numerical results by Sichov (1998) (•••) on the inner surface of the fixed edge of the cylindrical shell: growth of the Rabotnov damage parameter with time (a) and relaxation of the stress intensity (b).

the initial value of the time step $\Delta t_0 = 0.005$ h and with accuracy $\delta = 10^{-3}$ while $\omega \leqslant 0.9$. Numerical results have been obtained for discretization with 201 points in the radial direction and 17 points along the thickness of the plate. It was found that the damage variable reaches its critical value on the inner surface of the fixed edge of the circular plate, and the failure initiation time obtained for the plate under consideration in the present approach was equal to 175 h compared with 200 h in the calculations by Sichov (2003).

Thus, a good correlation is obtained between the creep damage patterns in the shells and its failure initiation time based on the present model, and other numerical model predictions existing in the literature as well as the experimental data available for the shell.

7. Conclusions

In this paper, a model for the numerical analysis of creep deformation and creep damage growth in thin branched shells of revolution under axisymmetrical loading is proposed. Constitutive equations for creep deformation associated with dislocation creep and the growth of parallel penny-shaped microcracks as well as the evolution equation for the damage variable are introduced in order to describe different properties of the material in tension and compression. The corresponding initial/boundary-value problem is formulated, and the combination of the fourth-order Runge–Kutta–Merson's method of time integration with automatic time step control together with the discrete orthogonal shooting method of Godunov is proposed in order to obtain the numerical solution. The predictions of the creep deformation and of the patterns of damage evolution with and without the tension–compression asymmetry of the material are given for a shell with non-branched meridian and for a branched shell. The numerical analysis has shown that in both cases the deflection growth, distribution of strains and stresses, and the creep damage evolution are essentially different when analyzed with and without tension asymmetry. This difference is obtained to be more significant for the branched shell. Therefore the consideration of the tension–compression asymmetry of the material is particularly necessary for the analysis of the creep deformation and the creep damage evolution in thin-walled branched shells. An assumption regarding identical behavior of the material in tension and compression leads to a significant underestimation of the failure initiation time of the branched shell. A good correlation is obtained between the creep damage patterns in the shells and its failure initiation time based on the present model, and other numerical model predictions existing in the literature as well as the experimental data available for the shell.

Acknowledgements

The research described in this paper is sponsored by the Alexander von Humboldt Foundation, Germany, the National Research Council of the USA and the Japan Society for the Promotion of Science (Long-Term Program).

References

Altenbach, H., Naumenko, K., 1997. Creep bending of thin-walled shells and plates by consideration of finite deflections. Comp. Mech. 19, 490–495.

Altenbach, H., Zolochevsky, A., 1991. Creep of thin shells in consideration of the anisotropic materials and the different behavior in tension and compression. Forsch. Ingenieurwesen 57, 172–179.

Altenbach, H., Altenbach, J., Zolochevsky, A., 1995. Erweiterte Deformationsmodelle und Versagenskriterien der Werkstoffmechanik. Deutscher Verlag für Grundstoffindustrie, Stuttgart.

Ashby, M.F., Brown, L.M., 1983. Perspectives in Creep Fracture. Pergamon, Oxford.

Bathe, K.J., 1996. Finite Elements Procedures. Prentice-Hall, Englewood Cliffs, NY.

Bellenger, E., Bussy, P., 2001. Phenomenological modeling and numerical simulation of different modes of creep damage evolution. Int. J. Solids Struct. 38, 577–604.

Betten, J., 2002. Creep Mechanics. Springer-Verlag, Berlin.

Betten, J., Borrmann, M., 1987. Stationäres Kriechverhalten innendruckbelasteter dünnwandiger Kreiszylinderschalten unter Berücksichtigung des orthotropen Werkstoffverhaltens und des CSD-Effects. Forsch. Ingenieurwesen 53, 75–82.

Betten, J., Sklepus, S., Zolochevsky, A., 1998. A creep damage model for initially isotropic materials with different properties in tension and compression. Eng. Fracture Mech. 59, 623–641.

Betten, J., Sklepus, S., Zolochevsky, A., 1999. A microcrack description of creep damage in crystalline solids with different behaviour in tension and compression. Int. J. Damage Mech. 8, 197–232.

Betten, J., Sklepus, A., Zolochevsky, A., 2003. A constitutive theory for creep behavior of initially isotropic materials sustaining unilateral damage. Mech. Res. Commun. 30, 251–256.

Boyle, J.T., Spence, J., 1983. Stress Analysis for Creep. Butterworths, London.

Chaboche, J.-L., Cailletaud, G., 1996. Integration methods for complex plastic constitutive equations. Comput. Methods Appl. Mech. Eng. 133, 125–155.

Chan, K.S., Lankford, J., Page, R.A., 1984. Viscous cavity growth in ceramics under compressive loads. Acta Metall. 32, 1907–1914.

Chen, I.W., Argon, A.S., 1981. Creep cavitation in 304 stainless steel. Acta Metall. 29, 1321–1333.

Chen, G.G., Hsu, T.R., 1988. A mixed explicit–implicit (El) algorithm for creep stress analysis. Int. J. Numerical Methods Eng. 26, 511–524.

Cocks, A.C.F., Ashby, M.F., 1982. Creep fracture by coupled power-law creep and diffusion under multiaxial stress. Met. Sci. 16, 465–474.

El-Shennawy, M., Morita, Y., Kouso, M., 1999. Analytical and experimental investigation for tensile and compressive creep of the A3003P aluminium alloy used for plate-fin heat exchanger. JSME Int. J. 42A, 403–413.

Evans, H.E., 1984. Mechanisms of Creep Fracture. Elsevier Applied Science, London.

Flügge, W., 1973. Stresses in Shells. Springer-Verlag, Berlin.

Godunov, S.K., 1961. Numerical solution of boundary value problems for systems of linear ordinary differential equations. Uspechi Mat. Nauk 16, 171–174.

Gorev, B.V., Rubanov, V.V., Sosnin, O.V., 1978. Creep of materials with different properties in tension and compression. In: Pisarenko, G.S. (Ed.), Strength of Materials and Structural Members under Multiaxial Loading. Naukova Dumka, Kiev, pp. 223–231.

Gorev, B.V., Rubanov, V.V., Sosnin, O.V., 1979. Construction of creep equations for materials with different properties in tension and compression. J. Prikl. Mech. Tech. Phys. (4), 121–128.

Grigolyuk, E.I., Shalashilin, V.I., 1991. Problems of Nonlinear Deformation: The Computational Method Applied to Nonlinear Problems in Solid Mechanics. Kluwer, Dordrecht.

Hayhurst, D.R., 1972. Creep rupture under multi-axial states of stress. J. Mech. Phys. Solids 20, 381–390.

Hayhurst, D.R., 1981. Discussion on the paper: ''Generalised structural models in creep mechanics'' by Boyle, J.T., Spence, J. In: Ponter, A.R.S., Hayhurst, D.R. (Eds.), Creep in Structures. Springer-Verlag, Berlin, p. 247.

Hayhurst, D.R., Dimmer, P.R., Chernuka, M.W., 1975. Estimates of the creep rupture lifetime of structures using the finite element method. J. Mech. Phys. Solids 23, 335–355.

Hayhurst, D.R., Trampczynski, W.A., Leckie, F.A., 1980. Creep rupture under non-proportional loading. Acta Metall. 28, 1171–1183.

Hayhurst, D.R., Dimmer, P.R., Morrison, G.J., 1984. Development of continuum damage in the creep rupture of notched bars. Trans. R. Soc. Lond. A 311, 103–129.

Hostert, B., 1975. Beitrag zum Kriechverhalten von Al 99,98 unter Druck-und Zugbeanspruchung. Ph.D. thesis, RWTH Aachen.

Hyde, T.H., Xia, L., Becker, A.A., 1996. Prediction of creep failure in aeroengine materials under multi-axial stress states. Int. J. Mech. Sci. 38, 385–403.

Hyde, T.H., Sun, W., Leen, S.B., Rayner, G., 2003. FE analysis of the creep of branched pipes, In: Banks, W.M., Nash, D.H. (Eds.), Proceeding of the Conference on Pressure Equipment Technology: Theory and Practice. Glasgow, pp. 41–66.

Kassner, M.E., Hayes, T.A., 2003. Creep cavitation in metals. Int. J. Plast. 19, 1715–1748.

Kawai, M., 2002. Constitutive modeling of creep and damage behaviors of the non-Mises type for a class of polycrystalline metals. Int. J. Damage Mech. 11, 223–246.

Kaz, Sh. N., 1955. Investigation of stress-rupture strength of pipes made from carbon steels. Teploenergetika 11, 37–40.

Khojasteh-Vahabzadeh, M.T., 1991. Beitrag zum Zug- und Druckkriechverhalten von Ti 99,9 und TiA16V4. Ph.D. thesis, RWTH Aachen.

Kojic, M., Bathe, K.J., 1987. Thermo-elastic-plastic and creep analysis of shell structures. Comput. Struct. 26, 135–143.

Kraus, H., 1980. Creep Analysis. John Wiley and Sons, NY.

Kumar, V., Morjaria, M., Mukherjee, S., 1980. Numerical integration of some stiff constitutive models of inelastic deformation. Trans. ASME. J. Eng. Mater. Technol. 102, 92–96.

Lemaitre, J., Chaboche, J.-L., 1990. Mechanics of Solid Materials. Cambridge University Press, Cambridge.

Ling, L., Tu, S.-T., Gong, J.-M., 2000. Application of Runge–Kutta–Merson algorithm for creep damage analysis. Int. J. Press. Vessel Piping 77, 243–248.

Lucas, G.E., Pelloux, R.M.N., 1981. Texture and stress state dependent creep in Zircaloy-2. Met. Trans. 12A, 1321–1331.

Mahnken, R., 2003. Creep simulation of asymmetric effects by use of stress mode dependent weighting functions. Int. J. Solids Struct. 40, 6189–6209.

Miuazaki, N., 1987. Creep buckling analysis of circular cylindrical shells under axial compression–bifurcation buckling analysis by the finite element method. Trans. ASME. J. Press. Vessel Technol. 109, 179–183.

Morachkovskii, O.K., Zolochevskii, A.A., 1980. Effect of initial orthotropy of material on the creep of shell structures. Sov. Appl. Mech. 16, 478–482.

Murakami, S., Liu, Y., 1995. Mesh-dependence in local approach to creep fracture. Int. J. Damage Mech. 4, 230–250.

Murakami, S., Liu, Y., Mizuno, M., 2000. Computational methods for creep fracture analysis by damage mechanics. Comput. Methods Appl. Mech. Eng. 183, 15–33.

Nechtelberger, E., 1985. Raumtemperaturkriechen und Spannungsabhängigkeit des E-Moduls von Graudußwerkstoffen. Osterr. Ing. Archit. Z. 130, 29–36.

Needleman, A., Rice, J.R., 1983. Plastic creep flow effects in the diffusive cavitation of grain boundaries. Acta Metall. 28, 1315–1332.

Nikitenko, A.F., Sosnin, O.V., Torshenov, N.G., Shokalo, I.K., 1971. Creep of hardening materials with different properties in tension and compression. J. Appl. Mech. Technol. Phys. 12, 277–281.

Ohashi, Y., Ohno, N., Kawai, M., 1982. Evaluation of creep constitutive equations for type 304 stainless steel under repeated multiaxial loading. Trans. ASME. J. Eng. Mat. Technol. 107, 1–6.

Page, R.A., Lankford, J., Spooner, S., 1984. Nucleation and early-stage growth of creep cavities in hot-pressed silicon carbide. Acta Metall. 32, 1275–1286.

Penny, R.K., Marriott, D.L., 1995. Design for Creep. Chapman and Hall, London.

Pintschovius, L., Gering, E., Munz, D., Fett, T., Soubeyroux, J.L., 1989. Determination of non-symmetric secondary creep behaviour of ceramics by residual stress measurement using neutron diffractometry. J. Mater. Sci. Lett. 8, 811–813.

Providakis, C.P., 2002. D/BEM implementation of Robinson's viscoplastic model in creep analysis of metals using a complex variable numerical technique. Adv. Eng. Softw. 33, 805–816.

Rabotnov, Yu.N., 1969. Creep Problems in Structural Members. North-Holland, Amsterdam.

Riedel, H., 1987. Fracture at High Temperatures. Springer-Verlag, Berlin.

Rix, K.F.W., 1997. Konstitutive Gleichungen für metallische Werkstoffe unter zeitveränderlicher Hochtemperatur-Beanspruchung. Ph.D. thesis, RWTH Aachen.

Rubanov, V.V., 1987. Experimental foundation of the constitutive equations of creep for materials with different behaviour in tension and compression. Ph.D. thesis, Siberian Branch of the Russian Academy of Sciences, Institute of Hydrodynamics, Novosibirsk.

Saanouni, K., Chaboche, J.L., Bathias, C., 1986. On the creep-crack growth predictions by a local approach. Eng. Fract. Mech. 25, 677–691.

Sakane, M., Tokura, H., 2002. Experimental study of biaxial creep damage for type 304 stainless steel. Int. J. Damage Mech. 11, 247–262.

Saleeb, A.F., Arnold, S.M., Castelli, M.G., Wilt, T.E., Graf, W., 2001. A general hereditary multimechanism-based deformation model with application to the viscoplastic response of titanium alloys. Int. J. Plast. 17, 1305–1350.

Shariyat, M., Eslami, M.R., 1996. Isoparametric finite-element thermoelasto-plastic creep analysis of shells of revolution. Int. J. Press. Vessel Piping 68, 249–259.

Sichov, A., 1998. Eine verbesserte Schalentheorie unter Einbeziehung geometrischer Nichtlinearität sowie der Schubverzerrungen in Problemen der Kriechmechanik. Journal of the National Technical University "Kharkov Polytechnic Institute" 17, 68–72.

Sichov, A., 2003. Creep analysis in thin shells taking into account damage, geometrical nonlinearity and shear. Ph.D. thesis, National Academy of Sciences of Ukraine, Institute of Mechanical Engineering Problems, Kharkov.

Simo, J.C., Hughes, T.J.R., 1998. Computational Inelasticity. Springer-Verlag, NY.

Sosnin, O.V., 1970. Creep in materials with different tension and compression behaviour. J. Appl. Mech. Technol. Phys. 11, 832–835.

Takezono, S., Fujioka, S., 1981. The creep of moderately thick shells of revolution under axisymmetrical load. In: Ponter, A.R.S., Hayhurst, D.R. (Eds.), Creep in Structures. Springer-Verlag, Berlin, pp. 128–143.

Tilly, G.P., Harrison, G.F., 1972. A comparison between the tensile and compressive creep behaviour of an 11 per cent chromium steel. J. Strain Anal. 7, 163–169.

Tsvelodub, I.Yu., 1991. The Stability Postulate and its Applications in Creep Theory of Metallic Materials. Institute of Hydrodynamics, Novosibirsk.

Tvergaard, V., 1984. On the creep constrained diffusive cavitation of grain boundary effects. J. Mech. Phys. Solids 32, 373–393.

Voyiadjis, G.Z., Zolochevsky, A., 2000. Thermodynamic modeling of creep damage in materials with different properties in tension and compression. Int. J. Solids Struct. 37, 3281–3303.

Wereszczak, A.A., Ferber, M.K., Kirkland, T.P., Barnes, A.S., Frome, E.L., Menon, M.N., 1999. Asymmetric tensile and compressive creep deformation of hot-isostatically-presses Y_2O_3-Doped-Si_3N_4. J. Eur. Ceramic Soc. 19, 227–237.

Zolochevskii, A.A., 1982. Allowance for differences in strain resistance in the creep of isotropic and anisotropic materials. J. Appl. Mech. Technol. Phys. 23, 591–596.

Zolochevskii, A.A., 1988. Effect of the type of loading on the creep of isotropic strain-hardening materials. Sov. Appl. Mech. 24, 185–191.

Zolochevskii, A.A., Morachkovskii, O.K., 1982. Investigation of the creep of thin-walled shells under nonstationary loading. Sov. Appl. Mech. 18, 807–810.

Zolochevsky, A.A., 1980. Allowance for differences in tension and compression for materials in the creep problems of shells. In: Dynamics and Strength of Machines, No. 32, Kharkov, pp. 8–13.

Zolochevsky, A.A., 1982. Creep of thin shells for materials with different behavior in tension and compression. Ph.D. thesis, Institute of Mechanical Engineering Problems, Kharkov.

Zolochevsky, A., 1991. Creep of isotropic and anisotropic materials with different behaviour in tension and compression. In: Zyczkowski, M. (Ed.), Creep in Structures. Springer-Verlag, Berlin, pp. 217–220.

Zolochevsky, A.A., Morachkovsky, O.K., 1978. Investigation of axisymmetric creep of shell structures. In: Dynamics and Strength of Machines, No. 27, Kharkov, pp. 8–13.

Zolochevsky, A.A., Morachkovsky, O.K., 1979. Investigation of stress-rupture strength of shell structures. In: Dynamics and Strength of Machines, No. 30, Kharkov, pp. 32–36.

Zolochevsky, A., Obataya, Y., 2001. Tension-compression asymmetry of creep and unilateral creep damage in aluminum for isothermal and nonisothermal processes. JSME Int. J. 44A, 100–108.

Zolochevsky, A., Voyiadjis, G.Z., 2005. Theory of creep deformation with kinematic hardening for materials with different properties in tension and compression. Int. J. Plast. 21, 435–462.